

***GenomeFingerprinter* and universal genome fingerprint analysis for systematic comparative genomics**

Yuncan Ai*, Hannan Ai, Fanmei Meng, Lei Zhao

State Key Laboratory for Biocontrol, School of Life Sciences, Sun Yat-sen University,
Guangzhou 510275, P. R. China

Lssayc@mail.sysu.edu.cn

* Corresponding Author:

Yuncan Ai

Ph.D., Professor, Principal Investigator

Lssayc@mail.sysu.edu.cn

State Key Laboratory for Biocontrol

School of Life Sciences

Sun Yat-sen University

Guangzhou 510275

P. R. China

Abstract

Background:

How to compare whole genome sequences at large scale has not been achieved via conventional methods based on pair-wisely base-to-base comparison; nevertheless, no attention was paid to handle in-one-sitting a number of genomes crossing genetic category (chromosome, plasmid, and phage) with farther divergences (much less or no homologous) over large size ranges (from Kbp to Mbp). It should be a priority to pursue comparative genomics at large scale based on geometrical analysis of sequence in the post-genomic era. However, even how to simply visualize a DNA sequence has been challenging for decades; little progress has been made to date.

Results:

We created a new method, *GenomeFingerprinter*, to unambiguously produce three-dimensional coordinates from a sequence, followed by one three-dimensional plot and six two-dimensional trajectory projections to illustrate whole genome fingerprints. We further developed a set of concepts and tools and thereby established a new method, universal genome fingerprint analysis. We demonstrated their applications through case studies on over a hundred of genome sequences. Particularly, we defined the total genetic component configuration (TGCC) (i.e., chromosome, plasmid, and phage) for describing a strain as a system, and the universal genome fingerprint map (UGFM) of TGCC for differentiating a strain as a universal system, as well as the systematic comparative genomics (SCG) for comparing in-one-sitting a number of genomes crossing genetic category in diverse strains. By using UGFM (I), UGFM-TGCC (II), and UGFM-TGCC-SCG (III), we compared a number of genome sequences with farther divergences (chromosome, plasmid, and phage; bacterium, archaeal bacterium, and virus) over large size ranges

(6Kbp~5Mbp), giving new insights into critical problematic issues in microbial genomics in the post-genomic era.

Conclusion:

This paper provided a new method for rapidly computing, geometrically visualizing, and intuitively comparing genome sequences at fingerprint level, and hence established a new method of universal genome fingerprint analysis for systematic comparative genomics.

Keywords

Genome fingerprint, fingerprint analysis, systematic comparative genomics, computational visualization, geometrical analysis

Introduction

By using conventional methods based on pair-wisely base-to-base comparison, how to compare whole genome sequences at large scale has not been achieved; nevertheless, no attention was paid to handle in-one-sitting a number of genomes crossing different genetic category (chromosome, plasmid, and phage) with farther divergences (less or no homologous among genetic components) over large size ranges (from Kbp to Mbp per sequence). It should be a priority to persue comparative genomics at large scale based on geometrical analysis of sequence in the post-genomic era. However, little progress has been made to date; even how to simply visualize a DNA sequence has been challenging for decades [1].

Pioneering works in computer reading and geometrical visualizing of DNA sequence had been tried in one-dimension [2, 3], two-dimensions (Z-curve) [4], and three-dimensions (H-curve) [5, 6]. However, those were valid only for 'static' modeling and visualizing. The 'dynamic' modeling and visualizing in a virtual reality environment had been studied [7, 8]. A comprehensive example was AND-viewer, which provided a three-dimensional way to dynamically sense the big picture of a large DNA sequence in a virtual reality environment by using sensor, instead of mouse or keyboard. This pioneering effort had made fantastic progress for human to mimic 3D visions to intuitively sense genome sequences [7, 8], but still there was no possibility of using the datasets created for visions to further explore real biological contexts.

The post-genomic era promoted demanding of data mining and robust reasoning with huge amount of genome sequences [1]. Comparative genomics was essential to retrieve and mine genome sequences, there were numerous conventional methods, which were divided into two types: algebraic approach [9, 10, 11, 12] and geometrical approach [13, 14].

Algebraic approach means that calculating dissimilarity, or similarity or identity are based on pair-wisely base-to-base comparison; the outputs of calculation are only used for visualization through graphic techniques, rather than for robust data mining and reasoning analysis. Of course, tools for genomic data visualization are still essential for end-users to explore, interpret, and manipulate data [1]. The most common tools were BLAST [9] and CLUSTALW [10], which were only for pair-wisely comparisons among a certain number of short fragments at gene level. Recently, a BLAST-based visualization tool, BRIG, was constructed for genome-wide comparison to create images of multiple circular genomes among a number of closely related bacteria strains [11]. The output image showed BLAST-similarity between a central reference sequence and other sequences in question as a set of concentric rings, where BLAST-matches were colored on a sliding scale indicating a defined percentage of BLAST-identity. It had great advantage over other common tools, like ACT [12], in terms of the numbers of genomes being handled simultaneously and the ways of comparing and presenting of images in-one-sitting. These features made it a versatile approach for visualizing a range of genomic data, but it still was only for visions. Mauve [14, 15] was widely used for comparing and visualizing a number of genomes of close relatives in linear forms, which combined algebraic calculation and graphic display. However, even with close relatives only, the number of genomes being calculated and displayed dramatically depended on computation constraints causing too much CPU time (at least $O(n^2)$ in time complexity) or memory overflow, which limited to a fewer genomes of close relatives to be compared at once time.

Geometrical approach means that both calculation and visualization are dynamic for geometrical analysis with the input and output re-useable. One promising example was Zplotter (in Z-curve method) calculating three-dimensional coordinates from a linear genome sequence. Those coordinates were used to create a three-dimensional

geometrical vision in a rough manner (as open Z-curve) for a given DNA sequence [16]. Hundreds of such visions for microbial genomes were collected as a database [17]. The Z-curve method (based on Zplotter) was not only used for simple visualization [16, 17], but also for geometrical analysis to further explore real contexts of biology [18, 19, 20, 21]. For example, two replication *ori* points in archaeal genomes were predicted by Z-curve method [22, 23] and confirmed later by wet experiments in other labs [24, 25], showing its promising. Z-curve method was widely used by researchers around the world and had promoted the progress in understanding of genomics, starting a new frontier in geometrical analysis of genome sequences. However, Zplotter algorithm had an inevitable limitation in misrepresentation of a genome sequence but with different cutting-points (explanations in the main text), which would not be suitable for creating unique genome fingerprints.

In this paper, we present a new method, called *GenomeFingerprinter*, to unambiguously produce three-dimensional coordinates from sequence, followed by one three-dimensional plot and six two-dimensional trajectory projections to illustrate whole genome fingerprints. We further develop a set of concepts and tools and thereby establish a new method called universal genome fingerprint analysis. We demonstrate their applications through case studies on over a hundred of genome sequences, giving new insights into critical problematic issues in microbial comparative genomics. We anticipate that our methods could be widely applicable to systematic comparative genomics in the post-genomic era [1].

Results

Mathematical model and three-dimensional coordinates

For geometrical visualization of a given genome sequence, the key step is how to get its three dimensional coordinates (x_n, y_n, z_n). To do this, the Z-curve [16] defined a coordinate (x_n, y_n, z_n) for each base in a linear genome sequence ($n=1, 2, \dots, N$; N is the sequence length) by the equation (0). It defined a unique Z-curve from a given linear sequence, and *vice versa*. Note, it was designed for a linear genome sequence and A_n, T_n, G_n, C_n were the sum of numbers for each of four base-type (A, T, G, C), respectively, counting from the first base to other bases before and including the n^{th} base in a linear sequence ($n=1, 2, \dots, N$). The calculations could be performed by using Zplotter program [16]. The main problem here was the ambiguousness of the “first base” due to cutting-point errors in deposited genome sequences (see explanations later).

$$\begin{cases} x_n = (A_n + G_n) - (C_n + T_n) \\ y_n = (A_n + C_n) - (G_n + T_n) \\ z_n = (A_n + T_n) - (C_n + G_n) \end{cases} \quad (0)$$

Here, we take the same definition as equation (0), but with different contents of A_n, T_n, G_n, C_n . To do that, we thus propose a new mathematic model, called *GenomeFingerprinter*, for geometrical visualization of a circular genome sequence. A circular sequence contains 40-bps (5'-3'):

ACACTGACGCACACTGACGCACACTGACGCACACTGACGC (Figure 1) as an artificial example will be used to illustrate the conceptual principals of our method.

Firstly, we randomly select a base (n^{th}) as the first target base (TB). For the given TB (n^{th}), we define its relative distances (RD) (1) to the other moving m^{th} base (as focusing base, FB) ($m=1, 2, \dots, N$).

$$RD_n^m = \begin{cases} 1, & (m = n + 1) \\ 2, & (m = n + 2) \\ \dots & \dots \\ N-1, & (m = n + n-1) \\ N, & (m = n + n) \end{cases} \quad (1)$$

Here, the RD concept is critical. Once we have selected the given TB (suppose at position 1, base **A**) and the other moving FB (suppose at position 20, base **C**), the RD value is 19 (Figure 1). Thus, a collection of RD values ($m=1, 2, \dots, N$) will be generated for the given TB. Particularly, the RD formula (1) can virtually treat an arbitrary linear sequence as a circular one. For example, when the moving m^{th} FB is located at the position of $n+n$, the RD is N , which means the RD value now is N , not zero, when the moving m^{th} FB going over one circle (i.e., starting from the position at the n^{th} base and finishing at the same position at the n^{th} base).

Secondly, we define the weighted relative distance (WRD) (2) (N is the sequence length). The example above will have value $19/40$. This is simply to reduce memory burden and thus release computation constraints for larger sequences.

$$WRD_n^m = \frac{RD_n^m}{N} \quad (2)$$

Thirdly, for the same chosen TB (n^{th}), we define the sum of the weighted relative distances (SWRD) (3) from the above collection of WRD ($m=1, 2, \dots, N$) for each of the four base-type (A, G, T, C), respectively.

$$\begin{aligned} SWRD_n^A &= \sum_n^A [WRD_n^m] \\ SWRD_n^G &= \sum_n^G [WRD_n^m] \\ SWRD_n^T &= \sum_n^T [WRD_n^m] \\ SWRD_n^C &= \sum_n^C [WRD_n^m] \end{aligned} \quad (3)$$

Fourthly, we define the coordinate (x_n, y_n, z_n) (4) for the chosen TB (n^{th}). Note, here we count the sum of the weighted relative distances (SWRD) (unlike Z-curve method counting the sum of numbers) for each of four base-type (A, T, G, C),

respectively. So far, that is only one cycle done for only one chosen TB (n^{th}).

$$\begin{cases} x_n = (\text{SWRD}_n^A + \text{SWRD}_n^G) - (\text{SWRD}_n^C + \text{SWRD}_n^T) \\ y_n = (\text{SWRD}_n^A + \text{SWRD}_n^G) - (\text{SWRD}_n^G + \text{SWRD}_n^T) \\ z_n = (\text{SWRD}_n^A + \text{SWRD}_n^T) - (\text{SWRD}_n^G + \text{SWRD}_n^G) \end{cases} \quad (4)$$

Finally, we will repeat the above cycle, i.e., selecting the next TB (e.g., $n=2$ here) and repeating the process. We will have total N cycles ($n=1, 2, \dots, N$); each cycle has only one chosen TB and creates only one coordinate (x_n, y_n, z_n) for that chosen TB. All N bases will have their coordinates (x_n, y_n, z_n) after having finished all of these N cycles. We have developed in-house script, GenomeFingerprinter.exe, to do all.

As an example, the artificial 40-bps genome sequence (Figure 1) had its coordinates (x_n, y_n, z_n) (Table 1), which were calculated by using our program GenomeFingerprinter.exe, giving each base with a coordinate (x_n, y_n, z_n) as a point in the three-dimensional space, in total 40 points for the whole sequence.

Three-dimensional plot (3D-P) and primary genome fingerprint map (P-GFM)

The three-dimensional coordinates (x_n, y_n, z_n) can be plotted out as a three-dimensional plot (3D-P) to give a geometrical vision. The artificial 40-bps sequence had only 40 points (Table 1) hence giving a naive vision. As real examples, we showed visions for fragmental sequences ranging from tens to hundreds of kilobases (Table 2) of *Escherichia coli* strains (Figure 2). Clearly, each vision had its unique genome fingerprint (GF) both globally and locally. We defined such a GF vision as genome fingerprint map (GFM). The GFM was an intuitive identity for an individual genome sequence, and vice versa. Therefore, from now on, we can directly operate and compare GFM for studying sequence. That is, we compare genome sequences through genome fingerprints (via geometrical analysis) instead of sequence base-pairs (via algebraic analysis). For convenience, we further defined the

three-dimensional plot vision as the primary genome fingerprint map (P-GFM).

Two-dimensional trajectory projections (2D-TPs) and secondary genome fingerprint maps (S-GFMs)

To demonstrate sophisticated genome fingerprints, we created six two-dimensional trajectory projections (2D-TPs) for a given P-GFM by combining different components from its coordinates, including $x_n \sim n$, $y_n \sim n$, $z_n \sim n$, $x_n \sim y_n$, $x_n \sim z_n$, and $y_n \sim z_n$. For convenience, we defined these six 2D-TPs as the secondary genome fingerprint maps (S-GFMs). For example, six S-GFMs of *Escherichia coli* K-12/W3110 genome sequence clearly showed subtle variations both globally and locally (Figure 3). Note that S-GFMs of $x_n \sim z_n$, $y_n \sim z_n$, $x_n \sim y_n$ beared much more sensitive information compared to those of $x_n \sim n$, $y_n \sim n$, and $z_n \sim n$, respectively. Generally, S-GFMs can amplify subtle variations that are insensitive or invisible in P-GFMs. Particularly, S-GFMs of $x_n \sim y_n$, $x_n \sim z_n$ and $y_n \sim z_n$ are much more sensitive in differentiating local subtle variations, intuitively identifying unique genome features; whereas S-GFMs of $x_n \sim n$, $y_n \sim n$ and $z_n \sim n$ are relatively less informative but useful when focusing on global patterns (Figure 3).

Universal genome fingerprint map (UGFM)

P-GFM and S-GFMs can be either separately or sequentially used. For convenience, we defined the universal genome fingerprint map (UGFM) to unify both of them. By UGFM, we could compare in-one-sitting a number of sequences and display their GFMs at once time, on which each GFM could be classified into different groups solely based on its location (Figure 4).

For example, six archaeal genomes and twelve fragmental sequences from *E.coli* strains (Table 2) had complex P-GFMs (Figure 4). Within the species *Sulfolobus*

islandicus, strains M.14.25 and M.16.4 shared global similarity in P-GFM (Figure 4, A), indicating subtle variations at strain level. However, with farther divergences, strain *S. islandicus* Y.N.15.51 globally differed from *Methanococcus voltae* A3 but locally shared similar regions in P-GFM (Figure 4, B); whereas *S. islandicus* Y.G.57.14 completely differed from *Methanosphaera stadtmanae* 3091 (Figure 4, C), confirming their farther lineages.

On the other hand, within the species *Sulfolobus islandicus*, two strains M.14.25 and M.16.4 had only subtle variations (Figure 4, A), how could they be precisely differentiated by P-GFM? We defined geometrical center ($\bar{x}, \bar{y}, \bar{z}$) as a distinctive indicator for a single P-GFM to compare individual P-GFMs. For example, two strains M.14.25 and M.16.4 had different geometrical center values (644.00, -2081.00, 388729.14) and (476.50, -1916.50, 387938.64), respectively, and hence were clearly distinguishable.

Furthermore, those twelve fragmental sequences from *E.coli* strains (Table 2, Figure 4, D) were further enlarged and displayed as a UGFM besides their own individual P-GFMs (Figure 5). Clearly, there were six groups on UGFM (Figure 5, A, B, C, D, E, F) solely based on the locations of different P-GFMs. Particularly, different fragmental sequences either from the same strain (e.g., 91.1.1, 91.1.61, 91.6.59) or from different strains (e.g., 913.5.57, 4431.1.70, 7946.4.7, 10473.1.74, 10498.4.86, 12947.1.50, 13941.2.60) (Table 2) could be revealed as complicated P-GFM patterns. Some were similar (91.1.61, 913.1.77 and 10473.1.74 (Figure 5, A); 91.6.59, 913.5.57 and 13941.2.60 (Figure 5, B)) but most were different (Figure 5, C, D, E, F) no matter what the lineage was, strongly demonstrating the facts that there were modular domains in these genomes and such mosaic structures probably remained their tracking of evolutionary history. Most interestingly, a given P-GFM had quite different

views between its own P-GFM and that on UGFM simply because of the scale-down and view-angle rotation effect in UGFM (Figure 5). This feature would ensure UGFM as a powerful tool for large-scale global comparison in-one-sitting among a large number of whole genome sequences, theoretically, as many sequences as possible as long as the computer memory could allow.

Universal genome fingerprint analysis (UGFA)

Now that we had such a powerful tool, UGFM, based on unambiguous genome fingerprints, to compare a large number of whole genome sequences in-one-sitting (Figure 5), we further established a new method called universal genome fingerprint analysis (UGFA) (Figure 6). We anticipated that UGFA would be effective for systematic comparative genomics at large scale by expanding the scope of genetic category in question. Briefly, the UGFA method consisted of three subcategories (Figure 6): UGFM (I) (Figure 7, 8, 9), UGFM-TGCC (II) (Figure 10), and UGFM-TGCC-SCG (III) (Figure 11) corresponding to three objects: a genome, a strain, and a set of strains, respectively. For each subcategory, demonstration with examples of case studies was described in details below.

UGFM (I): Universal genome fingerprint map (UGFM)

Firstly, UGFM (I) was the foundation and the first major component of our UGFA method. It was proved powerful in global comparison at large scale for prokaryote bacteria genomes (Figure 5). More examples were from a number of genomes of archaeal bacterium (Table 2, Figure 7), phage (Table 3, Figure 8), and virus (Table 3, Figure 9). Five archaeal bacteria strains (*Halomonas elongate* DSM 2581, *Halorhodospira halophila* SL1, *Halorhabdus utahensis* DSM 12940, *Halothermothrix orenii* H 168 and *Halothiobacillus neapolitanus* c2) representing five genera of halophilic Archaea were displayed as a UGFM (Figure 7) showing larger scale-down

and view-angle rotation effect. Clearly, each strain had only one chromosome with size ranging of 2.6 ~4.1 Mbp; and these five archaeal chromosomes had no close relationships at all (Figure 7) confirming their farther diverse lineages at genus level (Table 2,). However, forty seven phages of family *Microviridae* (Table 3) that were grouped into two major clusters (Figure 8) and twenty four coronavirus strains (Table 3) that were classified into seven clusters (Figure 9) perfectly matched to their biological identities among close relatives. Put together, these findings from total eight three genomes (i.e., twelve bacteria, five archaeal bacteria, forty seven phages, and twenty four viruses) as good examples demonstrated that UGFM (I) could apply to any genetic category (bacterium, archaeal bacterium, phage, and virus) no matter how farther (Figure 7) or closer (Figure 5, 8, 9) divergences of genetic components in comparison.

UGFM-TGCC (II): Universal genome fingerprint map (UGFM) of total genetic component configuration (TGCC)

Secondly, how to compare a number of genome sequences crossing different genetic category (e.g., chromosome, plasmid, and phage) in a strain? Accordingly, we defined the total genetic component configuration (TGCC) as a set of genomes crossing all genetic category (chromosome, plasmid, and phage, if applicable) in a strain for describing a strain as a system. We further defined the universal genome fingerprint map (UGFM) of total genetic component configuration (TGCC) (UGFM-TGCC) for differentiating a strain in view of a universal system. Therefore, we could use UGFM-TGCC (II) to compare in-one-sitting among all genetic components in a strain, regardless the format of category (chromosome, plasmid, and phage).

For example, four strains crossing four genera in haophilic Archaea (Table 2) including *Halogeometricum boringquense* DSM 11551 (one chromosome and five

plasmids), *Haloterrigena turkmenica* DSM 5511 (one chromosome and six plasmids), *Natrialba magadii* ATCC 43099 (one chromosome and three plasmids), *Natrinema pellirubrum* DSM 15624 (one chromosome and two plasmids) were demonstrated by UGFM-TGCC (II) (Figure 10) clearly indicating their farther lineages at genus level. Note that the scale-down and view-angle rotation effect revealed the farther divergences between one chromosome and multiple plasmids in a certain strain, suggesting that it would be challenging for conventional methods to compare them due to much less or no homologous. Specifically, in the same figure (Figure 10, H), the tiny green spot (plasmid NC_008213) and the giant red vision (chromosome NC_008212) with farther divergences would not be easily compared by any other conventional methods.

UGFM-TGCC-SCG (III): UGFM-TGCC-based systematic comparative genomics (SCG)

Thirdly, how to compare a number of genome sequences both crossing genetic category in a strain (chromosome, plasmid, and phage) and crossing a number of strains (a cluster of strains) as a system (i.e., in-one-sitting)? To compare a number of such diverse genomes in-one-sitting, we defined a concept of UGFM-TGCC-SCG (III), UGFM-TGCC-based systematic comparative genomics (SCG). Note, here we called it as “systematic comparative genomics (SCG)” simply because all genomes crossing different genetic category (chromosome, plasmid, and phage) among diverse strains should be much less or even no homologous at all, which would be incredibly challenging to any known conventional methods that principally based on similarity analysis of homologous. In other words, to our knowledge to date, no one conventional method could handle such farther diverse genetic components in-one-sitting; to which even no attention was paid before. In fact, all of the

documented researches on comparative genomics to date were automatically based on the assumption that there was so-called a reference genome sequence for very close relatives in question; otherwise, they would not bother to do comparison. But, in our case, we exactly focused on the opposites that had much less or even no homologous and compared those diverse genetic components crossing farther divergences regardless the format of genetic category and regardless the extent of lineage divergence. Therefore, we called our objects in comparison as the “systematic comparative genomics” in order to distinguish from other traditional routes. This was one of the core concepts and aims in the present study.

Indeed, our UGFM-TGCC-SCG (III) subcategory method was powerful to handle those extraordinary situations. For example, total nineteen genomes including six chromosomes and thirteen plasmids with larger size ranges (6Kbp ~ 4Mbp) could be, separately, mapped and analyzed by using UGFM-TGCC-SCG (III) (Figure 11). These nineteen genomes were from four strains crossing four genera of halophilic Archaea (Table 2) and analyzed in-one-sitting as two sets of comparison (Figure 11):

Halorubrum lacusprofundii ATCC 49239 (two chromosomes and one plasmid) vs.

Haloarcula marismortui ATCC 43049 (two chromosomes and seven plasmids);

Haloferax volcanii DS2 (one chromosome and four plasmids) vs. *Halomicrobium*

mukohataei DSM 12286 (one chromosome and one plasmid). Obviously, they were

certainly demonstrated as diverse lineages solely based on genome fingerprints. Most importantly, note that tiny spots (e.g., corresponding to 6Kbp) and giant ones (e.g., corresponding to 4Mbp) were harmoniously existed in the same figures (Figure 10, H, Figure 11, C), either closely or farther away. Such amazing landscapes could be only revealed by our unique methods under the notions of so-called “total genetic component configuration” and “systematic comparative genomics”, particularly, as UGFM-TGCC and UGFM-TGCC-SCG in these cases. These should be more than

enough as representatives to prove UGFM-TGCC-SCG (III) effective and powerful.

Case studies: Applications of universal genome fingerprint analysis (UGFA)

Objectives

As for more specific examples, we chose two archaeal halobacteria strains, *Halobacterium* sp. NRC-1 and *Halobacterium salinarum* R1 (Table 2) [26, 27], to pursue systematic comparative genomics by using our UGFA method. It was not only because they had incredible microbiological features such as genome-wide evolution events [28, 29] and multiple replication *ori* points (unlike the common prokaryotes with only one replication *ori* point) that could be easily tracking [23], but also because two genomes were independently sequenced by two labs [28, 29] and had led to interesting arguments about critical problematic issues in microbial genomics and taxonomy, such as whether they were the same species or strain [29] or their genome sequences were correctly assembled particularly considering of mega-plasmids or minichromosomes [30, 31], and what might be the mechanism for evolutions [29, 31, 32, 33], even what should be considered for refining a “species” in taxonomy [34]. We expected that the universal genome fingerprint analysis (UGFA) could provide new insights into these critical problematic issues that would be crucial and invaluable for modern microbiology in the post-genomic era.

Genome-wide evolution events

From the sophisticated genome fingerprints in S-GFMs (Figure 12), two deposited chromosomes NRC-1 (NC_002607) and R1 (NC_010364) were very similar but not identical having subtle differences at strain level (Figure 12, A, B, E, F), supporting the claim that two strains were virtually from the same ancestor but had undergone evolutions [31, 32]. The subtle variations (Figure 12, C, D, G) also indicated the

genome-wide evolution events (shown by arrow-markers), causing longer of NRC-1 chromosome. It was coincided with the documented facts that the IS-element-rich regions [27] shuttled between chromosomes and mega-plasmids [30, 31], but the core genes conserved [33].

Two replication ori points

Again, from S-GFMs, two replication *ori* points, *oriC1* and *oriC2*, (Figure 12, E, F, H) were identified and the replication domains in two genomes were demonstrated identical, and those evolution events were not located in such replication regions. These evidences also supported the claim that two strains virtually came from the same ancestor strain [31, 32]. Most interestingly, two replication *ori* points in strain NRC-1 were reported as the first representatives of archaeal bacteria, changing the traditional definition of only one *ori* point in prokaryotes. In fact, one of two *ori* points was predicted by theoretical Z-curve analysis [22, 23] and confirmed by biological experiments later [24, 25]. Thus the reproducibility in identification of such two replication *ori* points in two sequences has proved that our method is as effective and sensitive as Z-curve analysis [22, 23].

UGFM-TGCC-SCG for differentiating strains

Two strains NRC-1 and R1 were completely different in terms of the numbers of plasmids and total base-pairs (Table 4). How to concisely describe their differences in visualization remained challenging. For example, they had eight genetic components including two chromosomes and six plasmids (Table 4), which made it ambiguous to only compare any part of them as traditional comparative genomics did. We thus should compare all of eight genomes in order to differentiate two strains unambiguously. By using UGFM-TGCC-SCG (Figure 13), we compared eight genome sequences with farther divergences crossing different genetic category (i.e.,

chromosome and plasmid) over large size ranges (40Kb ~ 3Mb) (Table 4) that would be challenging for conventional methods. In short, the UGFM-TGCC-SCG vision clearly confirmed that two strains were completely different and eight components had farther divergences (Figure 13, B). Particularly, two chromosomes were almost the same (Figure 13, B) but six plasmids had larger divergences (Figure 13, A), strongly indicating that plasmids had no close lineages with chromosomes in two strains. In addition, two mega-plasmids in strain NRC-1 had no close lineages with four plasmids in strain R1, suggesting there was no possibility to misassemble them due to less homologous. Most interestingly, even within the same strain, chromosome and plasmid showed distinctive lineage divergences. In other words, there was no correlation between chromosome and plasmid within a certain strain (i.e., no binding to a certain strain), indicating possible independent evolution among chromosomes and plasmids.

Double-check between UGFM-TGCC-SCG and Mauve

To double-check the lineages revealed by UGFM-TGCC-SCG (Figure 13), we used progressiveMauve mode [14] analysis to make pair-wisely multiple genome alignment among eight components (Figure 14, A) showing overall bare homologous although it took much longer time; whereas Mauve mode [15] analysis failed in such a comparison because it stopped alignment due to no essential homologous, as we predicted beforehand. Mauve mode [15] analysis yet worked well, separately, with subsets of six plasmids (Figure 14, B) and two chromosomes (Figure 14, C), respectively, and confirmed those partial relationships among six plasmids and between two chromosomes. We thus concluded that the lineage relationships revealed by UGFM-TGCC-SCG could be partially confirmed by Mauve method and confirmed that two strains were completely different and remained as sister-strains

within one species. In other words, in this case, progressiveMauve mode [14] could barely compatible to UGFM-TGCC-SCG (III) whereas Mauve mode [15] did not, but it could be used to deal with subsets, separately.

Discussion

As mentioned before, how to compare whole genome sequences at large scale has not been achieved by using conventional methods [11, 14] that based on pair-wisely base-to-base sequence similarity analysis; even no attention was paid to handle in-one-sitting a number of genomes crossing different genetic category with farther divergences (e.g., less or no homologous among crossing genetic components: chromosome, plasmid, and phage; bacterium, archaeal bacterium, and virus) over large size ranges (e.g., from Kbp to Mbp per genome sequence). We believe that how to pursue comparative genomics at large scale based on geometrical analysis of sequence, rather than pair-wisely base-to-base comparison, will be a priority in the post-genomic era. However, little progress has been made to date, even how to visualize a DNA sequence has been challenging for decades [1]. To our knowledge to date, no method for creating “unambiguous genome fingerprint (GF)” was documented; no concept of “universal genome fingerprint analysis (UGFA)”, or “total genetic component configuration (TGCC)”, or “systematic comparative genomics (SCG)” was proposed. Particularly, note that all sequences of components both crossing different genetic category (e.g., chromosome, plasmid, and phage; bacterium, archaeal bacterium, and virus) and crossing a number of diverse strains in-one-sitting should be much less or no homologous at all, which would be incredibly challenging to any known conventional methods that principally based on pair-wisely base-to-base homologous analysis. No conventional method could handle

in-one-sitting such farther diverse genetic components. Therefore, it would be impossible to compare our methods, *GenomeFingerprinter* and universal genome fingerprint analysis (UGFA), as a whole system with other documented methods in terms of advantages and disadvantages. However, in the present study, we tried best to compare partial features with two programs partly related to ours.

***GenomeFingerprinter* vs. Zplotter**

Validity

Zplotter (in Z-curve method as a geometrical-type approach) was mainly used to create coordinates for subsequent use by Z-curve analysis, but not used for what we proposed as creating the “genome fingerprint (GF)” and the “universal genome fingerprint analysis (UGFA)” in the present study. Although Zplotter’s coordinates were used to produce hundreds of graphs (as Z-curves) of microbial genomes documented as a database [17], there were no stable features in terms of so-called fingerprints. In fact, for example, we re-plotted visions for *Halobacterium* sp. NRC-1 genome sequence [NC_002607] by using Zplotter’s coordinates of either z_n' (Figure 15, B) or z_n (Figure 15, C) to present as an open rough Z-curve. Note that those visions themselves created by using z_n' and z_n , respectively, were quite different from each other due to wavelet transform in the algorithm of Zplotter [16]. In contrast, our method presented a unique circular vision with accurate and delicate fingerprint for the same genome (Figure 15, A). Also note that using z_n' (Figure 15, B) showed a similar frame of vision to ours except that it was in an open rough Z-curve with lesser features whereas using z_n (Figure 15, C) gave a complete different vision from ours. We thus recommend that our *GenomeFingerprinter* method could be an alternate of Zplotter to provide more accurate and delicate coordinates for Z-curve analysis, but should be aware of choosing whether z_n from our method or z_n' from Zplotter, referring

to the specific questions for various researches.

Reliability

Furthermore, we had found a major problem when using Zplotter to handle circular genome sequences with cutting-point errors. In fact, Zplotter was designed for a linear sequence [16] because its algorithm depends on counting the absolute numbers of bases starting from the “first” base in a given linear sequence. In fact, when a deposited sequence as a linear form (i.e., no matter what the original form should be as either linear or circular), even the same circular sequence with cutting-point errors changing its real “first” base could be quite different for the input to Zplotter so that the output visions were differently presented (Figure 15, B, C). In contrast, our method was initially created for a circular sequence (Figure 1), but it could apply to a linear form since linear one would be a specific form of circular one and particularly because our method measured the relative distance in a circular form (as discussed with the formula (1) before, Figure 1), rather than the absolute numbers of bases counting from the “first” base in a linear sequence. For example, the same circular sequence *Halobacterium* sp. NRC-1 (NC_002607) with different cutting-point (e.g., NC_002607_RC re-cut at 700 kbps) were incorrectly presented as different visions by using Zplotter’s coordinates (Figure 15, B, C), whereas the exact same vision was shown by our method (Figure 15, A). Thus our method was valid for both circular and linear forms and no matter where the cutting-point was.

Adaptability

Finally, we would like to address the fundamental scientific principals for why dealing with circular genomes should be critical for microbes. That was overlooked in literatures before.

Theoretically, the circular form [32] would be much more stable than its linear form in living cells. In nature, most microbial genomes are in circular double strands, which protect them from natural degradation because of relatively simple structure. Also, the circular genomes and their linear forms are usually changing into each other only when they are living at certain functioning stages, such as rolling-model replication and plasmid-mediated conjunction. Most importantly, circular and linear forms are functioning both genetically and physiologically in a coordinated way for a given genome in a given microbe. In other words, their forms are changeable into each other only when responding to real living conditions [32, 33]. Anyway, we could catch up the circular form status in life cycles.

Technically, the techniques and people in different groups were not yet unified to guarantee all deposited genome sequences in correct forms. In fact, most sequences deposited in public databases so far were neither in their natural orders of starting from the real “first” base, nor in the direction from 5' to 3'. We thus had to tackle with such cutting-point errors, as illustrated by examples (Figure 15). Fortunately, as mentioned before, the RD formula (1) in our method could virtually treat an arbitrary linear sequence as a circular one (Figure 1), avoiding the impact of any possible cutting-point errors existed in public deposited sequences.

Informatively, the closed (or in circular form) fingerprint beared much more information, concerning with genome-wide comparative genomics at fingerprint level (Figure 12, 13). Most importantly, our method was initially designed for circular forms (Figure 1), but finally was proved not ambiguous for linear forms when dealing with cutting-point errors (Figure 15). In other words, our method could precisely calculate the three-dimensional coordinates for a given circular or linear sequence with or without correct cutting-point, could accordingly present a unique genome fingerprint

giving a certain geometrical center $(\bar{x}, \bar{y}, \bar{z})$ (Figure 15), and could consequently guarantee the subsequent unambiguous trajectory projections. In short, our method guaranteed the validity of universal genome fingerprint analysis.

To sum up, we conclude that *GenomeFingerprinter* has advantages over Zplotter in creating unambiguous coordinates and therefore can be an alternate component of Z-curve method, which can be widely applicable to all aspects established by Z-curve method to date [18, 19, 20, 21, 22, 23] and beyond.

GenomeFingerprinter vs. Mauve

Efficiency

Mauve (as an typical algebraic-type program), combined computing and plotting in-one-sitting, is commonly used for pair-wisely comparison and vision [14]. However, it had difficulty with a number of larger genome sequences due to its inner constraints, either too slow or memory overflow (MO). In contrast, our method could rapidly calculate and visualize, separately, tens of large genomes. For example, Mauve had at least $O(n^2)$ whereas our method had $O(n)$ in time complexity (Table 5). By using our method, only if plotting all larger graphics in-one-sitting would cause memory overflow. Examples were five bacterial chromosome genomes (Figure 7), forty seven phage genomes (Figure 8), and twenty four virus genomes (Figure 9), respectively, that could be easily plotted out in-one-sitting. Particularly, our method calculated and visualized, separately, and thus not only ensured the higher performance efficiency for large set of genomes (Table 5) but also offered both inputs and outputs re-usable for the subsequent processes of universal genome fingerprint analysis and beyond (e.g., for Z-curve analysis consequently).

On the other hand, Mauve had two modes: progressiveMauve mode [14] and

Mauve mode [15]. As discussed before, only progressiveMauve mode [14] could partially deal with what we so-called systematic comparative genomics (Figure 14, A) showing overall bare homologous although it took much longer time; whereas Mauve mode [15] failed in the comparison because it stopped alignment due to no essential homologous. Mauve mode [15] analysis yet worked well, separately, with subsets of six plasmids (Figure 14, B) and two chromosomes (Figure 14, C), respectively, and confirmed those partial relationships among six plasmids and between two chromosomes.

Prediction

Mauve [14, 15] can visualize what it is, but can not predict what it should be without a reference sequence or specific pre-knowledge. In contrast, our method provides geometrical analysis of genome fingerprints with six trajectory projections, which intuitively predict unique features such as genome-wide evolution events and replication *ori* points (Figure 12), either based on a reference sequence or derived from common knowledge.

Compatibility

From universal genome fingerprint analysis (UGFA), the subtle variations (Figure 12, C, D, G) could predict genome-wide evolution events at small scale in chromosomes, but no direct evidence yet could be drawn. Thus we used Mauve to pair-wisely compare two genomes and confirmed genome-wide evolution events (Figure 12, C), demonstrating that our method can rapidly predict evolution events and Mauve can precisely test and confirm such predictions by showing out the predicted specific regions (Figure 12, C). The same was true for UGFM-TGCC-SCG by our method (Figure 13) and the pair-wisely comparison by progressiveMauve (Figure 14, A). Thus, we recommend that our method and Mauve method are compatible and partners,

taking both advantages of our method for rapid and intuitive prediction in general and Mauve for slow and precise confirmation in details, particularly focusing on the targeted fragments' gain, lose, and rearrangement, etc..

To conclude, methodologically, the universal genome fingerprint analysis (UGFA) through UGFM-TGCC-SCG (Figure 13) and the pair-wisely genome comparison through Mauve (Figure 14) could be compatible in a manner of sequential operations. In other words, the UGFM-TGCC-SCG method not only could handle exceptional situations for a large set of genomes, but also could facilitate the efficiency of integrating Mauve into performing our so-called systematic comparative genomics, particularly, in terms of in-one-sitting for a set of sequences with farther divergences (chromosome, plasmid, and phage, if applicable) over large size ranges (e.g., 6Kbp ~ 4Mbp). In other words, any component with too farther divergence could be rapidly pre-screened out by UGFM-TGCC-SCG, which could guide on the selection of appropriate subsets of components for subsequent comparison by Mauve.

Prospective in future for universal genome fingerprint analysis

Genome fingerprints and the concepts of strain and species

“Strain” should be the most fundamental unit for taxonomy. The concise definition of type strain should be crucial for assigning type species, type genus, type family and beyond. Any deep conflicts in arguable strains would eventually shape the assigned species or beyond. Unfortunately, it was so critical but had been overlooked by literatures. To our knowledge to date, no efficient method could provide full description about a type strain, nor was there common agreement upon how to define a species [26, 34, 35]. We anticipated that genomics would be the solid foundation for these issues, as it had re-constructed the concepts of numbers - two or more instead of only one - of chromosomes and replication *ori* points. For example, in the present study, by

using our method *GenomeFingerprinter*, we created the whole genome fingerprints (Figure 12, 13) for all eight genetic components in two arguable strains (Table 4) and fundamentally demonstrated that they were not identical (Figure 12, 13) and should probably belong to the same species that needed more characterizations yet. These findings supported the proposal that genome sequence information should be considered in refining an arguable “strain” or “species” in the taxonomy of halophilic Archaea [34]. We agreed with the promotion that in the long run, the definition for a “species” in modern microbiology needed intensive revisions in light of genomics to unify inevitable conflicts in nomenclature system, particularly, in halophilic Archaea [34, 35]. We would further recommend that all genetic components should be included when referring to genomic information for discussing unambiguous taxonomy although to what extent chromosome, plasmid and phage plays roles, respectively, still remained unclear and to be negotiated at current knowledge level [26, 34, 35]. We believed that using UGFM-TGCC-SCG method to concisely resolve the arguments between closely related strains (Figure 13) as well as among farther divergence species or genera (Figure 10, 11, 12, 13) would be one of the crucial steps forwarding to modern microbial nomenclature in the post-genomic era.

Type UGFM-TGCC fingerprint for type strain

We would recommend that any arguable strains should not be judged identical or different only based upon partial information from bulky traditional features such as phenotype and genotype including 16S rRNA, AFLP, PCR-RFLP, ISs, MITEs, etc. [26, 27, 31, 34]. It should also be true for defining a type strain. Theoretically, we would define a type strain or name a new isolate or refine an arguable strain or construct a refined-version for modern microbial taxonomy based upon all unambiguous information from total genome sequences (i.e., chromosome, plasmid, and phage, if

applicable). Practically, at least, a type strain should have a meaningful genomic signature. For example, the UGFM-TGCC fingerprint (Figure 10, 11, 12, 13) would be effective to provide a “type strain” with a “type UGFM-TGCC fingerprint” which is simple, standard, and meaningful.

Interestingly, to date, the list of genomes sequenced does not include that of the type strain of *Halobacterium salinarum* (ATCC 33171), the type species of the type genus of the family and the order [36]. It is regretted that no genomic information is available for the nomenclatural type [36]. We expect the community should consider of sequencing more type strains in order to set up a solid foundation for refining modern Archaea taxonomy, which would be invaluable for the next generation of community to understand deeply, research systematically and use efficiently of such amazing bio-resources. Once the “type genome sequence” for the “type strain” is available, the “type UGFM-TGCC fingerprint” can be made by using our methods, as what we did for two related strains *Halobacterium* NRC-1 and *Halobacterium salinarum* R1 (Figure 13) and five diverse strains crossing five genera (Figure 10).

Overall, the family *Halobacteriaceae* consisted of 36 genera with 129 species standing in nomenclature (as of November 2011) [26], but only sixteen strains representing sixteen genera had been sequenced and deposited in GenBank (as of February 2013), including eighteen chromosomes and thirty-six plasmids (Table 2). By using our method of UGFM (I), UGFM-TGCC (II), and UGFM-TGCC-SCG (III), we created the whole genome fingerprints (Figure 10, 11, 12, 13) for all fifty-four genome sequences. Our results provided new insights into critical problematic issues in halophilic Archaea genomics, comparative genomics, and taxonomy [26, 34]. That was a great step on initiatives. We expected more pioneering works to be done. In short, the present paper provided a new method (*GenomeFingerprinter*, Figure 1) for

rapidly computing, geometrically visualizing, and intuitively comparing sequences at fingerprint level, and hence established a new method (universal genome fingerprint analysis (UGFA), Figure 6) for systematic comparative genomics, which would be invaluable for the first strategic step forwarding to microbial genomics, comparative genomics, phylogenetics, and taxonomy in the light of post-genomics. We anticipated that our methods could be widely applicable to systematic comparative genomics.

Conclusions

We created a new method, *GenomeFingerPrinter*, to unambiguously produce three-dimensional coordinates from a sequence, followed by one three-dimensional plot and six two-dimensional trajectory projections to illustrate whole genome fingerprints. We further developed a set of concepts and tools (3D-P, 2D-TP, GF, GFM, P-GFM, S-GFM, UGFM, TGCC, UGFM-TGCC, SCG, and UGFM-TGCC-SCG), and thereby established a new method, universal genome fingerprint analysis (UGFA). We demonstrated their applications through case studies on over a hundred of genome sequences. Particularly, by using UGFM (I), UGFM-TGCC (II), and UGFM-TGCC-SCG (III), we compared a number of genome sequences crossing different genetic category (chromosome, plasmid, and phage; bacterium, archaeal bacterium, and virus) with farther divergences over large size ranges (6Kbp~5Mbp), which we called as systematic comparative genomics, giving new insights into critical problematic issues in microbial genomics. We anticipated that our methods could be widely applicable to systematic comparative genomics in the post-genomic era.

Materials

Genome sequences used in this study were downloaded from NCBI or were derived from this study were list in Table 2, 3.

Methods

We implemented our method into an in-house script, GenomeFingerprinter.exe. It will be available upon request to the corresponding author. Zplotter (v1.0) and Mauve (v2.3.1) used in this study can be downloaded from links: Zplotter.exe at <http://tubic.tju.edu.cn/zcurve/> and Mauve at <http://gel.ahabs.wisc.edu/mauve/>. To plot graphics from coordinates, any public graphic tool can be used.

Abbreviations

bps: base pairs; Kbp: kilo-bps; Mbp: Mega-bps; TB: target base; FB: focusing base; RD: relative distance; WRD: weighted relative distance; SWRD: sum of the weighted relative distances; 3D-P: three-dimensional plot; 2D-TP: two-dimensional trajectory projections; GF: genome fingerprint; GFM: genome fingerprint map; P-GFM: primary genome fingerprint map; S-GFM: secondary genome fingerprint map; UGFM: universal genome fingerprint map; TGCC: total genetic component configuration; UGFM-TGCC: universal genome fingerprint map of total genetic component configuration; SCG: systematic comparative genomics; UGFM-TGCC-SCG: universal genome fingerprint map of total genetic component configuration based systematic comparative genomics; UGFA: universal genome fingerprint analysis

Acknowledgements

This work was supported by National High Technology Research & Development Project (2006AA09Z420), National Science and Technology Major Project of China (2011ZX08011005) grants to YA. HA was a recipient of Guangzhou Municipal Science Ambassador Scholarship.

Authors' contributions

Conceived and designed the experiments: YA and FM. Performed experiments: LZ (Perl) and HA (Perl and Java) initiated models and scripts; HA reconstructed mathematic models and algorithms, designed, implemented, tested scripts, and constructed system; YA, FM and HA initiated, developed and confined the conceptual frameworks for biological research contents; HA and YA performed computing and collected data. Analyzed the data: HA, YA and FM. Wrote the paper: YA, HA and FM.

Competing interests

The author(s) declare that they have no competing interests.

References

1. Nielsen CB, Cantor M, Dubchak I, Gordon D, Wang T. (2010) Visualizing genomes: techniques and challenges. *Nat Methods* 7(Suppl 3): S5-S15.
2. Lathe R, Findlay R. (1984) Machine-readable DNA sequences. *Nature* 311: 610.
3. Lathe R, Findlay R. (1985) Reply. *Nature* 314: 585-586.
4. Gates MA. (1986) A simple way to look at DNA. *J Theor Biol* 119: 319-328.
5. Hamori E, Ruskin J. (1983) H-Curves, a novel method of representation of nucleotide series especially suited for long DNA sequences. *J Biol Chem* 258: 1318-1327.
6. Hamori E. (1985) Novel DNA sequence representations. *Nature* 314: 585.
7. Herisson J, Ferey N, Gros P.E, Gherbi R. (2006) ADN-viewer: A 3D approach for bioinformatic analyses of large DNA sequences. *Cellular Mol Biol* 52: 24-31.
8. Herisson J, Payen G, Gherbi R. (2007) A 3D pattern matching algorithm for DNA

- sequences. *Bioinformatics* 23: 680-686.
9. Altschul S, Madden TL, Schaffer AA, Zhang J, Zhang Z, Miller W, Lipman DJ. (1997) Gapped BLAST and Psi-BLAST: A new generation of protein database search programs. *Nucl Acids Res* 25: 3389-3402.
 10. Thompson JD, Higgins DG, Gibson TJ. (1994) CLUSTALW: improving the sensitivity of progressive multiple sequence alignment through sequence weighting, positions specific gap penalties and weight matrix choice. *Nucleic Acids Res* 22:4673-4680.
 11. Alikhan NF, Petty NK, Ben Zakour NL, Beatson SA. (2011) BLAST Ring Image Generator (BRIG): simple prokaryote genome comparisons. *BMC Genomics* 12:402.
 12. Carver TJ, Rutherford KM, Berriman M, Rajandream MA, Barrell BG, Parkhill J. (2005) ACT: The artemis comparison tool. *Bioinformatics* 21: 3422-3423.
 13. Lobry JR. (1996) A simple vectorial representation of DNA sequences for the detection of replication origins in bacteria. *Biochimie* 78: 323-326.
 14. Aaron E, Darling, Bob Mau, Nicole T. Perna. (2010) progressiveMauve: Multiple genome alignment with gene gain, loss, and rearrangement. *PLoS One* 5: e11147.
 15. Darling ACE, Mau B, Blatter FR, Perna NT. (2004) Mauve: multiple alignment of conserved genomic sequence with rearrangements. *Genome Research* 14: 1394-1403.
 16. Zhang R, Zhang CT. (1994) Z Curves, An intuitive tool for visualizing and analyzing the DNA sequences. *J Biomol Struc Dynamics* 11: 767-782.

17. Zhang CT, Zhang R, Ou HY. (2003) The Z curve database: a graphic representation of genome sequences. *Bioinformatics* 19: 593-599.
18. Guo FB, Ou HY, Zhang CT. (2003) ZCURVE: a new system for recognizing protein-coding genes in bacterial and archaeal genomes. *Nucleic Acids Res* 31: 1780-1789.
19. Zheng WX, Chen LL, Ou HY, Gao F, Zhang CT. (2005) Coronavirus phylogeny based on a geometric approach. *Mol Phy and Evo* 36: 224-232.
20. Zhang CT, Gao F, Zhang R. (2005) Segmentation algorithm for DNA sequences. *Phys Rev E* 72: 041917.
21. Gao F, Zhang CT. (2006) GC-Profile: a web-based tool for visualizing and analyzing the variation of GC content in genomic sequences. *Nucleic Acids Res* 34(Web Server issue):W686-W691.
22. Zhang R, Zhang CT. (2002) Single replication origin of the archaeon *Methanosarcina mazei* revealed by the Z curve method. *Biochem Biophys Res Commun* 297: 396-400.
23. Zhang R, Zhang CT. (2003) Multiple replication origins of the archaeon *Halobacterium* species NRC-1. *Biochem Biophys Res Commun* 302: 728-734.
24. Charkowski AO. (2004) Making sense of an alphabet soup: the use of a new bioinformatics tool for identification of novel gene islands. *Physiol Genomics* 16: 180-181.
25. Robinson NP, Dionne I, Lundgren M, Marsh VL, Bernander R, Bell SD. (2004) Identification of two origins of replication in the single chromosome of the Archaeon *Sulfolobus solfataricus*. *Cell* 116: 25-38.

26. Oren, A. (2012) Taxonomy of the family *Halobacteriaceae*: a paradigm for changing concepts in prokaryote systematics. *Int J Syst Evol Microbiol* 62:263-271.
27. File'e J, Siguier P, Chandler M. (2007) Insertion sequence diversity in Archaea. *Microbiol Mol Biol Rev* 71:121-157.
28. Ng WV, Kennedy SP, Mahairas GG, Berquist B, Pan M, Shukla HD, Lasky SR, Baliga NS, Thorsson V, Sbrogna J, Swartzell S, Weir D, Hall J, Dahl TA, Welti R, Goo YA, Cruz R, Danson MJ, Hough DW, Maddocks DG, Jablonski PE, Krebs MP, Angevine CM, Dale H, Isenbarger TA, Peck RF, Pohlschroder M, Spudich JL, Jung KW, Alam M, Freitas T, Hou S, Daniels CJ, Dennis PP, Omer AD, Ebhardt H, Lowe TM, Liang P, Riley M, Hood L, DasSarma S. (2000) Genome sequence of *Halobacterium* species NRC-1. *Proc Natl Acad Sci USA* 97:12176-12181.
29. Pfeiffer F, Schuster SC, Broicher A, Falb M, Palm P, Rodewald K, Ruepp A, Soppa J, Tittor J, Oesterhelt D. (2008) Evolution in the laboratory: the genome of *Halobacterium salinarum* strain R1 compared to that of strain NRC-1. *Genomics* 91: 335-346.
30. Berquist BR, DasSarma S. (2003) An archaeal chromosomal autonomously replicating sequence element from an extreme halophile, *Halobacterium* sp. strain NRC-1. *J Bacteriol* 185: 5959-5966.
31. Ng WV, Ciufo SA, Smith TM, Bumgarner RE, Baskin D, Faust J, Hall B, Loretz C, Seto J, Slagel J, Hood L, DasSarma S. (1998) Snapshot of a large dynamic replicon in a halophilic archaeon: megaplasmid or minichromosome? *Genome Res* 8: 1131-1141.
32. Kennedy SP, Ng WV, Salzberg SL, Hood L, DasSarma S. (2001) Understanding

- the adaptation of *Halobacterium* species NRC-1 to its extreme environment through computational analysis of its genome sequence. *Genome Res* 11:1641-1650.
33. Capes MD, DasSarma P, DasSarma S. (2012) The core and unique proteins of haloarchaea. *BMC Genomics* 13:39.
 34. DasSarma P, DasSarma S. (2008) On the origin of prokaryotic "species": the taxonomy of halophilic Archaea. *Saline Systems* 4:5.
 35. Oren, A. (2008) Nomenclature and taxonomy of halophilic archaea – comments on the proposal by DasSarma and DasSarma for nomenclatural changes within the order *Halobacteriales*. *Int J Syst Evol Microbiol* 58: 2245–2246.
 36. Oren A, Arahal DR, Ventosa A. (2009) Emended descriptions of genera of the family *Halobacteriaceae*. *Int J Syst Evol Microbiol* 59:637-642.

Figures and Legends

Figure 1. A mathematic model for getting coordinates (x_n , y_n , z_n) from a circular genome sequence. It is arbitrarily starting at the n^{th} base as the chosen target base (TB) and moving to the m^{th} base as a focusing base (FB).

Figure 2. Three-dimensional plot (3D-P) and primary genome fingerprint map (P-GFM) of fragmental genome sequences of chromosomes in *Escherichia coli* strains. (A). K-12/W3110 [AC_000091]F7; (B). BL21(DE3)pLysS AG [NC_012947]F1; (C). BL21(DE3)pLysS AG [NC_012947]F5; (D). O55:H7/CB 9615 [NC_013941]F1.

Figure 3. Six two-dimensional trajectory projections (2D-TP) and secondary genome fingerprint maps (S-GFMs) for *E. coli* K-12/W3110 chromosome [AC_000091]. (A). Projection with $x_n \sim n$; (B). Projection with $y_n \sim n$; (C). Projection with $z_n \sim n$; (D). Projection with $x_n \sim y_n$; (E). Projection with $x_n \sim z_n$; (F). Projection with $y_n \sim z_n$.

Figure 4. Universal genome fingerprint map (UGFM) for overall comparison of genome fingerprints. (A). Similar: *Sulfolobus islandicus* M.14.25 [NC_012588] and M.16.4 [NC_012726]; (B). Partly similar: *S. islandicus* Y.N.15.51 [NC_012623] and *Methanococcus voltae* A3 [NC_014222]; (C). Different: *S. islandicus* Y.G.57.14 [NC_012622] and *Methanosphaera stadtmanae* 3091 [NC_007681]; (D). Mixture: (total twelve fragmental sequences (Table 2): 91.1.1, 91.1.61, 91.6.59, 913.1.77, 913.5.57, 4431.1.70, 7946.4.7, 10473.1.74, 10473.4.57, 10498.4.86, 12947.1.50,

13941.2.60.

Figure 5. Application of universal genome fingerprint map (UGFM) for comparison among a number of genomes in-one-sitting. The twelve fragmental genome sequences (list in Table 2) were shown in UGFM. The primary genome fingerprint map (P-GFM) of each sequence was classified into different groups solely based upon its location in UGFM: Group (A) (91.1.61, 913.1.77 and 10473.1.74), Group (B) (91.6.59, 913.5.57 and 13941.2.60), Group (C) (7946.4.7 and 12947.1.50), Group (D) (10498.4.86), Group (E) (91.1.1), and Group (F) (4431.1.70). Note that each sequence showed quite different views between its own P-GFM and that in UGFM simply because of the scale-down and view-angle rotation effect in UGFM, which ensured for larger number of objects to be compared in-one-sitting.

Figure 6. Diagram of conceptual framework for universal genome fingerprint analysis (UGFA). Our methods consisted of *GenomeFingerprinter* and universal genome fingerprint analysis (UGFA); the former was the fundamental for the latter. The objects could be a single genome sequence, or a number of genome sequences crossing different genetic category (e.g., chromosome, plasmid, phage) in a strain, or a number of sequences of genetic components in a cluster of strains crossing different genetic category (e.g., bacterium, archaeal bacterium, virus). The UGFA method was composed by three subcategories of UGFM (I), UGFM-TGCC (II), and UGFM-TGCC-SCG (III), corresponding to the above three objects, respectively. The core lied in the systematic concepts and tools, which included 3D-P, 2D-TP, P-GFM, S-GFM, UGFM, TGCC, UGFM-TGCC, SCG, and UGFM-TGCC-SCG. Abbreviations: 3D-P: three-dimensional plot; 2D-TP: two-dimensional trajectory projections; GF:

genome fingerprint; GFM: genome fingerprint map; P-GFM: primary genome fingerprint map; S-GFM: secondary genome fingerprint map; UGFM: universal genome fingerprint map; TGCC: total genetic component configuration; UGFM-TGCC: universal genome fingerprint map of total genetic component configuration; SCG: systematic comparative genomics; UGFM-TGCC-SCG: universal genome fingerprint map of total genetic component configuration based systematic comparative genomics; UGFA: universal genome fingerprint analysis

Figure 7. UGFM (I) of five archaeal strains (each having only one chromosome with size ranging of 2.6 ~4.1 Mbp) crossing five genera of halophilic Archaea.

Halomonas elongate DSM 2581 [NC_014532], *Halorhodospira halophilia* SL1 [NC_008789], *Halorhabdus utahensis* DSM 12940 [NC_013158], *Halothermothrix orenii* H 168 [NC_011899] and *Halothiobacillus neapolitanus* c2 [NC_013422] had no close lineages confirming their divergences, at genus level.

Figure 8. UGFM (I) of forty seven genomes of phages in the family of

***Microviridae*.** These forty seven phages were close relatives, but most of them were distinguishable at strain level. They were grouped into two major clusters. Cluster (1) included twenty nine strains (WA5, ID11, WA3, WA2, ID41, NC10, WA6, ID12, NC13, NC2, NC6, ID52, ID8, G4, ID2, WA14, ID18, WA45, ID21, NC28, ID62, NC35, NC29, NC3, alpha3, WA13, phiK, ID32, NC19); Cluster (2) included eighteen strains (NC16, NC5, NC37, ID1, NC7, NC1, NC11, ID22, S13, phiX174, WA11, WA4, ID34, NC41, NC56, WA10, NC51, ID45). The details of phage names were list in Table 3.

Figure 9. UGFM (I) of twenty four genomes of coronavirus strains. They were classified into seven clusters. Cluster (1) included the most similar twelve strains of SARS coronavirus ([AY283796], [AY283797], [AY283798], [AY283794], [AY291451], [AY278741], [AY283795], [AY278488], [AY278491], [AY278554], [NC_004718], [AY282752]), tracking with the same UGFM; Cluster (2) included similar four strains of Murine hepatitis virus ([AF201929], [AF208066], [AF208067], [NC_001846]), tracking with the similar UGFM; Cluster (3) was a distinctive Porcine epidemic diarrhea virus strain ([NC_003436]); Cluster (4) was a distinctive Avian infectious bronchitis virus strain ([NC_001451]); Cluster (5) was a distinctive Feline infectious peritonitis virus strain ([NC_002306]); Cluster (6) was a distinctive Human coronavirus strain ([NC_002645]); Cluster (7) included four similar strains of Bovine coronavirus ([AF220295], [u00735], [AF391542], [NC_003045]), tracking with the similar UGFM. These seven clusters were perfectly matched to their biological identity groups (list in Table 3).

Figure 10. UGFM-TGCC (II) of five archaeal strains crossing four genera of halophilic Archaea. (A) enlarged vision of those five plasmids and (B) *Halogeometricum boringquense* DSM 11551 (one chromosome [NC_014729] and five plasmids pHBOR02 [NC_014731], pHBOR04 [NC_014732], pHBOR01 [NC_014735], pHBOR03 [NC_014736], pHBOR05 [NC_014737]); (C) enlarged vision of those six plasmids and (D) *Haloterrigena turkmenica* DSM 5511 (one chromosome [NC_013743] and six plasmids pHTUR01 [NC_013744], pHTUR02 [NC_013745], pHTUR03 [NC_013746], pHTUR04 [NC_013747], pHTUR05 [NC_013748], pHTUR06 [NC_013749]); (E) enlarged vision of those three plasmids and (F) *Natrialba magadii* ATCC 43099 (one chromosome [NC_013922] and three plasmids

pNMAG01 [NC_013923], pNMAG02 [NC_013924], pNMAG03 [NC_013925]; (G) *Natrinema pellirubrum* DSM 15624 (one chromosome [NC_019962] and two plasmids pNATPE02 [NC_019963], pNATPE01 [NC_019967]; (H) *Haloquadratum walsbyi* DSM 16790 (one chromosome [NC_008212] and one plasmid PL47 [NC_008213]. These four strains crossing four genera (Table 2) had quite different UGFM-TGCC visions demonstrating their farther lineages at genus level.

Figure 11. UGFM-TGCC-SCG (III) of four archaeal strains (each having multiple chromosomes and plasmids) crossing four genera of halophilic Archaea. There were two sets of in-one-sitting comparison. One set (A-B) : *Halorubrum lacusprofundii* ATCC49239 (chromosome I [NC_012029], chromosome II [NC_012028], plasmid pHLAC01 [NC_012030]) vs. *Haloarcula marismortui* ATCC43049 (chromosome I [NC_006396], chromosome II [NC_006397], and seven plasmids pNG100 [NC_006389], pNG200 [NC_006390], pNG300 [NC_006391], pNG400 [NC_006392], pNG500 [NC_006393], pNG600 [NC_006394], pNG700 [NC_006395]) focusing on plasmids (A) and a universal system (B); Another set (C-D): *Haloferax volcanii* DS2 [chromosome [NC_013967], plasmid pHV3 [NC_013964], pHV2 [NC_013965], pHV4 [NC_013966], pHV1 [NC_013968]) vs. *Halomicrobium mukohataei* DSM 12286 (chromosome [NC_013202], plasmid pHmuk01[NC_013201]) focusing on plasmids (C) and a universal system (D).

Figure 12. Application of universal genome fingerprint analysis (UGFA) for comparative genomics between two chromosomes of *Halobacterium* sp. NRC-1 [NC_002607] and *Halobacterium salinarum* R1 [NC_010364]. Two arguable strains were compared by using three-dimensional plots ($x_n \sim y_n \sim z_n$) (P-GFM) (A) and

two-dimensional trajectory projections (S-GFM) with different combinations of coordinates: (B) $x_n \sim y_n$; (C) $x_n \sim z_n$; (D) $y_n \sim z_n$; (E) $x_n \sim n$; (F) $y_n \sim n$; (G) $z_n \sim n$; (H) $x_n \sim n$ and $y_n \sim n$ together. Note two arrows showed replication *ori* points, *ori*C1 and *ori* C2; other arrows indicated genome-wide evolution events.

Figure 13. Application of universal genome fingerprint analysis (UGFA) for systematic comparative genomics (SCG). The universal genome fingerprint map (UGFM) of total genetic component configurations (TGCC) (UGFM-TGCC) was applied to the systematic comparative genomics (SCG) in-one-sitting. Two strains *Halobacterium* sp. NRC-1 and *Halobacterium salinarum* R1 were compared as a universal system. (A). UGFM-TGCC-SCG for total six plasmids (*Halobacterium* sp. NRC-1 pNRC100 [NC_00001869] and pNRC200 [NC_002608]; *Halobacterium salinarum* R1 PHS1 [NC_010366], PHS2 [NC_010369], PHS3 [NC_010368], and PHS4 [NC_010367]); (B). UGFM-TGCC-SCG for those total six plasmids and two chromosomes (*Halobacterium* sp. NRC-1 [NC_002607] and *Halobacterium salinarum* R1 [NC_010364]). Note, even within the same strain, chromosome and plasmid showed distinctive lineage divergences. In other words, there was no correlation between chromosome and plasmid within a certain strain, i.e., without any binding to a certain strain, indicating possible independent evolution among chromosomes and plasmids.

Figure 14. Mauve snapshots for pair-wisely genome comparisons between two strains *Halobacterium* sp. NRC-1 and *Halobacterium salinarum* R1 considering of TGCC as a universal system. progressiveMauve mode analysis could compare in-one-sitting all eight components of NRC-1 and R1 strains showing bare

homologous (A). Mauve mode analysis failed because it stopped alignment due to no homologous; but it worked well, separately, with (B) six plasmids (the inner window) (*Halobacterium* sp. NRC-1 pNRC100 [NC_00001869] and pNRC200 [NC_002608]; *Halobacterium salinarum* R1 PHS1 [NC_010366], PHS2 [NC_010369], PHS3 [NC_010368], and PHS4 [NC_010367]), and (C) two chromosomes (*Halobacterium* sp. NRC-1 [NC_002607] and *Halobacterium salinarum* R1 [NC_010364]). Mauve mode analysis could clearly reveal the relationships among six plasmids and between two chromosomes, separately.

Figure 15. Comparisons between two chromosomes of *Halobacterium* sp. NRC-1 [NC_002607] and its derivative form (NC_002607_RC) with different cutting-point. (A). Comparison via *GenomeFingerPrinter*; (B). Comparison via Zplotter with z_n' ; (C). Comparison via Zplotter with z_n .

Tables and Captions

Table 1. Coordinates of an artificial sample sequence

# bp / point	x_n	y_n	z_n
1	0.7	8.1	-4.1
2	-0.3	8.7	-4.9
3	0.7	9.3	-3.7
4	-0.3	9.9	-4.5
5	-1.3	8.5	-3.3
6	-0.3	7.1	-4.1
7	0.7	7.7	-2.9
8	-0.3	8.3	-3.7
9	0.7	6.9	-4.5
10	-0.3	7.5	-5.3
11	0.7	8.1	-4.1
12	-0.3	8.7	-4.9
13	0.7	9.3	-3.7
14	-0.3	9.9	-4.5
15	-1.3	8.5	-3.3
16	-0.3	7.1	-4.1
17	0.7	7.7	-2.9
18	-0.3	8.3	-3.7
19	0.7	6.9	-4.5
20	-0.3	7.5	-5.3
21	0.7	8.1	-4.1
22	-0.3	8.7	-4.9
23	0.7	9.3	-3.7
24	-0.3	9.9	-4.5
25	-1.3	8.5	-3.3
26	-0.3	7.1	-4.1
27	0.7	7.7	-2.9
28	-0.3	8.3	-3.7
29	0.7	6.9	-4.5
30	-0.3	7.5	-5.3
31	0.7	8.1	-4.1
32	-0.3	8.7	-4.9
33	0.7	9.3	-3.7
34	-0.3	9.9	-4.5
35	-1.3	8.5	-3.3
36	-0.3	7.1	-4.1
37	0.7	7.7	-2.9
38	-0.3	8.3	-3.7
39	0.7	6.9	-4.5
40	-0.3	7.5	-5.3

Table 2. Features of genome sequences from bacteria and archaeal bacteria used in this study

Species and Strain	Sequence ID	Type	Size (bps)
Downloaded from FTP.ncbi.nlm.nih.gov [GenBank]			
<i>Escherichia coli</i> K-12/W3110	AC_000091	Chromosome*	4646332
	NC_007779		
<i>Escherichia coli</i> K-12/DH10B	NC_010473	Chromosome*	4686137
<i>Escherichia coli</i> K-12/MG1655	NC_000913	Chromosome*	4639675
<i>Escherichia coli</i> BL21 (DE3) pLysSAG	NC_012947	Chromosome*	4570938
<i>Escherichia coli</i> O55:H7/CB9615	NC_013941	Chromosome*	5386352
<i>Escherichia coli</i> UT189	NC_007946	Chromosome*	5065741
<i>Escherichia coli</i> CFT073	NC_004431	Chromosome*	5231428
<i>Escherichia coli</i> SMS-3-5	NC_010498	Chromosome*	5068389
<i>Sulfolobus islandicus</i> M.14.25	NC_012588	Chromosome*	2608832
<i>Sulfolobus islandicus</i> M.16.4	NC_012726	Chromosome*	2586647
<i>Sulfolobus islandicus</i> Y.N.15.51	NC_012623	Chromosome*	2812165
<i>Sulfolobus islandicus</i> Y.G.57.14	NC_012622	Chromosome*	2702058
<i>Methanococcus voltae</i> A3	NC_014222	Chromosome*	1936387
<i>Methanospaera stadmanae</i> DSM 3091	NC_007681	Chromosome*	1767403
<i>Halomonas elongate</i> DSM 2581	NC_014532	Chromosome ^{*,a}	4119315
<i>Halorhodospira halophila</i> SL1	NC_008789	Chromosome ^{*,a}	2716716
<i>Halorhabdus utahensis</i> DSM 12940	NC_013158	Chromosome ^{*,a}	3161321
<i>Halothermothrix orenii</i> H 168	NC_011899	Chromosome ^{*,a}	2614977
<i>Halothiobacillus neapolitanus</i> c2	NC_013422	Chromosome ^{*,a}	2619785
<i>Halogeometricum boringquense</i> DSM 11551	NC_014729	Chromosome ^{*,b}	2860838
<i>Halogeometricum boringquense</i> DSM 11551	NC_014731	plasmid pHBOR02 ^b	343853
<i>Halogeometricum boringquense</i> DSM 11551	NC_014732	plasmid pHBOR04 ^b	197618
<i>Halogeometricum boringquense</i> DSM 11551	NC_014735	plasmid pHBOR01 ^b	367369
<i>Halogeometricum boringquense</i> DSM 11551	NC_014736	plasmid pHBOR03 ^b	213355
<i>Halogeometricum boringquense</i> DSM 11551	NC_014737	plasmid pHBOR05 ^b	17786
<i>Haloterrigena turkmenica</i> DSM 5511	NC_013743	Chromosome ^{*,b}	3944596
<i>Haloterrigena turkmenica</i> DSM 5511	NC_013744	plasmid pHTUR01 ^b	708474
<i>Haloterrigena turkmenica</i> DSM 5511	NC_013745	plasmid pHTUR02 ^b	419558
<i>Haloterrigena turkmenica</i> DSM 5511	NC_013746	plasmid pHTUR03 ^b	183364
<i>Haloterrigena turkmenica</i> DSM 5511	NC_013747	plasmid pHTUR04 ^b	174400
<i>Haloterrigena turkmenica</i> DSM 5511	NC_013748	plasmid pHTUR05 ^b	72078
<i>Haloterrigena turkmenica</i> DSM 5511	NC_013749	plasmid pHTUR06 ^b	16041
<i>Natrialba magadii</i> ATCC 43099	NC_013922	Chromosome ^{*,b}	3805456
<i>Natrialba magadii</i> ATCC 43099	NC_013923	plasmid pNMAG01 ^b	383753
<i>Natrialba magadii</i> ATCC 43099	NC_013924	plasmid pNMAG02 ^b	258593
<i>Natrialba magadii</i> ATCC 43099	NC_013925	plasmid pNMAG03 ^b	59323
<i>Natrinema pellirubrum</i> DSM 15624	NC_019962	Chromosome ^{*,b}	3844629
<i>Natrinema pellirubrum</i> DSM 15624	NC_019963	plasmid pNATPE02 ^b	279762
<i>Natrinema pellirubrum</i> DSM 15624	NC_019967	plasmid pNATPE01 ^b	291912
<i>Haloquadratum walsbyi</i> DSM 16790	NC_008212	Chromosome ^{*,b}	3177244
<i>Haloquadratum walsbyi</i> DSM 16790	NC_008213	plasmid PL47 ^b	47537
<i>Halorubrum lacusprofundii</i> ATCC49239	NC_012029	Chromosome I ^{*,c}	2774371
<i>Halorubrum lacusprofundii</i> ATCC49239	NC_012028	Chromosome II ^{*,c}	533457
<i>Halorubrum lacusprofundii</i> ATCC49239	NC_012030	plasmid pHLAC01 ^c	437500
<i>Haloarcula marismortui</i> ATCC43049	NC_006396	Chromosome I ^{*,c}	3176463
<i>Haloarcula marismortui</i> ATCC43049	NC_006397	Chromosome II ^{*,c}	292165
<i>Haloarcula marismortui</i> ATCC43049	NC_006389	plasmid pNG100 ^c	33779
<i>Haloarcula marismortui</i> ATCC43049	NC_006390	plasmid pNG200 ^c	33930
<i>Haloarcula marismortui</i> ATCC43049	NC_006391	plasmid pNG300 ^c	40086
<i>Haloarcula marismortui</i> ATCC43049	NC_006392	plasmid pNG400 ^c	50776
<i>Haloarcula marismortui</i> ATCC43049	NC_006393	plasmid pNG500 ^c	134574
<i>Haloarcula marismortui</i> ATCC43049	NC_006394	plasmid pNG600 ^c	157519
<i>Haloarcula marismortui</i> ATCC43049	NC_006395	plasmid pNG700 ^c	416420
<i>Halomicrobium mukohataei</i> DSM 12286	NC_013202	Chromosome ^{*,c}	3154923
<i>Halomicrobium mukohataei</i> DSM 12286	NC_013201	plasmid pHmuk01 ^c	225032
<i>Haloferax volcanii</i> DS2	NC_013967	Chromosome ^{*,c}	2888440
<i>Haloferax volcanii</i> DS2	NC_013964	plasmid pHV3 ^c	444162
<i>Haloferax volcanii</i> DS2	NC_013965	plasmid pHV2 ^c	6450

<i>Haloferax volcanii</i> DS2	NC_013966	plasmid pHV4 ^c	644869
<i>Haloferax volcanii</i> DS2	NC_013968	plasmid pHV1 ^c	86308
<i>Halobacterium</i> sp.NRC-1	NC_002607	Chromosome ^{*d}	2014239
<i>Halobacterium</i> sp.NRC-1	NC_001869	Plasmid pNRC100 ^d	191346
<i>Halobacterium</i> sp.NRC-1	NC_002608	Plasmid pNRC200 ^d	365425
<i>Halobacterium salinarum</i> R1	NC_010364	Chromosome ^{*d}	2000962
<i>Halobacterium salinarum</i> R1	NC_010366	Plasmid PHS1 ^d	147625
<i>Halobacterium salinarum</i> R1	NC_010369	Plasmid PHS2 ^d	194963
<i>Halobacterium salinarum</i> R1	NC_010368	Plasmid PHS3 ^d	284332
<i>Halobacterium salinarum</i> R1	NC_010367	Plasmid PHS4 ^d	40894

Derivatives created in this study [based on those sequences from GenBank]

<i>Escherichia coli</i> K-12/W3110-91.1.1	91.1.1	Chromosome fragment	227694
<i>Escherichia coli</i> K-12/W3110-91.1.61	91.1.61	Chromosome fragment	324260
<i>Escherichia coli</i> K-12/W3110-91.6.59	91.6.59	Chromosome fragment	410186
<i>Escherichia coli</i> K-12/W3110-91.F7	91.7	Chromosome fragment	953958
<i>Escherichia coli</i> K-12/MG1655-913.1.77	913.1.77	Chromosome fragment	331163
<i>Escherichia coli</i> K-12/MG1655-913.5.57	913.5.57	Chromosome fragment	408963
<i>Escherichia coli</i> CFT073-4431.1.70	4431.1.70	Chromosome fragment	401260
<i>Escherichia coli</i> UTI89-7946.4.7	7946.4.7	Chromosome fragment	518065
<i>Escherichia coli</i> K-12/DH10B -10473.1.74	10473.1.74	Chromosome fragment	325622
<i>Escherichia coli</i> K-12/DH10B -10473.4.57	10473.4.57	Chromosome fragment	412818
<i>Escherichia coli</i> SMS-3-5-10498.4.86	10498.4.86	Chromosome fragment	331536
<i>Escherichia coli</i> BL21 (DE3) pLysSAG-12947.F1	12947.1	Chromosome fragment	1759795
<i>Escherichia coli</i> BL21 (DE3) pLysSAG-12947.1.50	12947.1.50	Chromosome fragment	470050
<i>Escherichia coli</i> BL21 (DE3) pLysSAG-12947.F5	12947.5	Chromosome fragment	43254
<i>Escherichia coli</i> O55:H7/CB9615-13941.F1	13941.1	Chromosome fragment	1915479
<i>Escherichia coli</i> O55:H7/CB9615-13941.2.60	13941.2.60	Chromosome fragment	267039

* 32 chromosomes used for calculations as list in Table 5.

^aUGFM (I): five strains and five genomes (Figure 7)

^bUGFM-TGCC (II): five strains and twenty two genomes (Figure 10)

^cUGFM-TGCC-SCG (III): four strains and nineteen genomes (Figure 11)

^dCase studies: two strains and eight genomes (Figure 12, 13, 14)

Table 3. Features of genome sequences from viruses and phages used in this study

Species and Strain	Sequence ID	Type	Size (bps)
Downloaded from FTP.ncbi.nlm.nih.gov [GenBank]			
WA5: Coliphage WA5	NC_007847	Phage chromosome ^a	5737
ID11: Coliphage ID11	NC_006954	Phage chromosome ^a	5737
WA3: Coliphage WA3	NC_007845	Phage chromosome ^a	5700
WA2: Coliphage WA2	NC_007844	Phage chromosome ^a	5700
ID41: Coliphage ID41	NC_007851	Phage chromosome ^a	5737
NC10: Coliphage NC10	NC_007854	Phage chromosome ^a	5687
WA6: Coliphage WA6	NC_007852	Phage chromosome ^a	5687
ID12: Coliphage ID12	NC_007853	Phage chromosome ^a	5687
NC13: Coliphage NC13	NC_007849	Phage chromosome ^a	5737
NC2: Coliphage NC2	NC_007848	Phage chromosome ^a	5737
NC6: Coliphage NC6	NC_007855	Phage chromosome ^a	5687
ID52: Coliphage ID52	NC_007825	Phage chromosome ^a	5698
ID8: Coliphage ID8	NC_007846	Phage chromosome ^a	5700
G4: Enterobacteria phage G4	NC_001420	Phage chromosome ^a	5737
ID2: Coliphage ID2	NC_007817	Phage chromosome ^a	5644
WA14: Coliphage WA14	NC_007857	Phage chromosome ^a	5644
ID18: Coliphage ID18	NC_007856	Phage chromosome ^a	5644
WA45: Coliphage WA45	NC_007822	Phage chromosome ^a	6242
ID21: Coliphage ID21	NC_007818	Phage chromosome ^a	6242
NC28: Coliphage NC28	NC_007823	Phage chromosome ^a	6239
ID62: Coliphage ID62	NC_007824	Phage chromosome ^a	6225
NC35: Coliphage NC35	NC_007820	Phage chromosome ^a	6213
NC29: Coliphage NC29	NC_007827	Phage chromosome ^a	6439
NC3: Coliphage NC3	NC_007826	Phage chromosome ^a	6273
alpha3: Enterobacteria phage alpha3	DQ085810	Phage chromosome ^a	6177
WA13: Coliphage WA13	NC_007821	Phage chromosome ^a	6242
phiK: Coliphage phiK	NC_001730	Phage chromosome ^a	6263
ID32: Coliphage ID32	NC_007819	Phage chromosome ^a	6245
NC19: Coliphage NC19	NC_007850	Phage chromosome ^a	5737
NC16: Coliphage NC16	NC_007836	Phage chromosome ^a	5540
NC5: Coliphage NC5	NC_007833	Phage chromosome ^a	5540
NC37: Coliphage NC37	NC_007837	Phage chromosome ^a	5540
ID1: Coliphage ID1	NC_007828	Phage chromosome ^a	5540
NC7: Coliphage NC7	NC_007834	Phage chromosome ^a	5540
NC1: Coliphage NC1	NC_007832	Phage chromosome ^a	5540
NC11: Coliphage NC11	NC_007835	Phage chromosome ^a	5540
ID22: Coliphage ID22	NC_007829	Phage chromosome ^a	5540
S13: Enterobacteria phage S13	NC_001424	Phage chromosome ^a	5540
phiX174: Coliphage phiX174	NC_001422	Phage chromosome ^a	5540
WA11: Coliphage WA11	NC_007843	Phage chromosome ^a	5541
WA4: Coliphage WA4	NC_007841	Phage chromosome ^a	5540
ID34: Coliphage ID34	NC_007830	Phage chromosome ^a	5540
NC41: Coliphage NC41	NC_007838	Phage chromosome ^a	5540
NC56: Coliphage NC56	NC_007840	Phage chromosome ^a	5540
WA10: Coliphage WA10	NC_007842	Phage chromosome ^a	5540
NC51: Coliphage NC51	NC_007839	Phage chromosome ^a	5540
ID45: Coliphage ID45	NC_007831	Phage chromosome ^a	5540
SARS coronavirus TW1	AY283796	Virus chromosome ^b	30137
SARS coronavirus Sin2679	AY283797	Virus chromosome ^b	30132
SARS coronavirus Sin2748	AY283798	Virus chromosome ^b	30137
SARS coronavirus Sin2774	AY283794	Virus chromosome ^b	30137

<i>SARS coronavirus</i> Sin2500	AY291451	Virus chromosome ^b	30155
<i>SARS coronavirus</i> Urbani	AY278741	Virus chromosome ^b	30153
<i>SARS coronavirus</i> Sin2677	AY283795	Virus chromosome ^b	30131
<i>SARS coronavirus</i> BJ01	AY278488	Virus chromosome ^b	30151
<i>SARS coronavirus</i> HKU-39849	AY278491	Virus chromosome ^b	30168
<i>SARS coronavirus</i> CUHK-W1	AY278554	Virus chromosome ^b	30162
<i>SARS coronavirus</i>	NC_004718	Virus chromosome ^b	30178
<i>SARS coronavirus</i> CUHK-Su10	AY282752	Virus chromosome ^b	30162
<i>Murine hepatitis virus</i> strain 2	AF201929	Virus chromosome ^b	31724
<i>Murine hepatitis virus</i> strain Penn 97-1	AF208066	Virus chromosome ^b	31558
<i>Murine hepatitis virus</i> strain ML-10	AF208067	Virus chromosome ^b	31681
<i>Murine hepatitis virus</i> strain A59	NC_001846	Virus chromosome ^b	31806
<i>Porcine epidemic diarrhea virus</i>	NC_003436	Virus chromosome ^b	28435
<i>Avian infectious bronchitis virus</i>	NC_001451	Virus chromosome ^b	28004
<i>Feline infectious peritonitis virus</i>	NC_002306	Virus chromosome ^b	29776
<i>Human coronavirus</i> 229E	NC_002645	Virus chromosome ^b	27709
<i>Bovine coronavirus</i> strain Quebec	AF220295	Virus chromosome ^b	31546
<i>Bovine coronavirus</i> strain Mebus	u00735	Virus chromosome ^b	31477
<i>Bovine coronavirus</i> isolate BCoV-LUN	AF391542	Virus chromosome ^b	31473
<i>Bovine coronavirus</i>	NC_003045	Virus chromosome ^b	31473

^aUGFM (I): forty seven strains and forty seven genomes in phage (Figure 8)

^bUGFM (I): twenty four strains and twenty four genomes in virus(Figure 9)

Table 4. Features of total genetic component configurations of strains NRC-1 and R1

Components	NRC-1	R1
Chromosome	NC_002607	NC_010364
(bp)	2014239	2000962
Plasmid 1	pNRC100	PHS1
(bp)	NC_001869	NC_010366
	191346	147625
Plasmid 2	pNRC200	PHS2
(bp)	NC_002608	NC_010369
	365425	194963
Plasmid 3		PHS3
(bp)	-	NC_010368
		284332
Plasmid 4		PHS4
(bp)	-	NC_0103667
		40,894
Total (bp)	2571010	2668776

Table 5. *GenomeFingerprinter* vs. Mauve

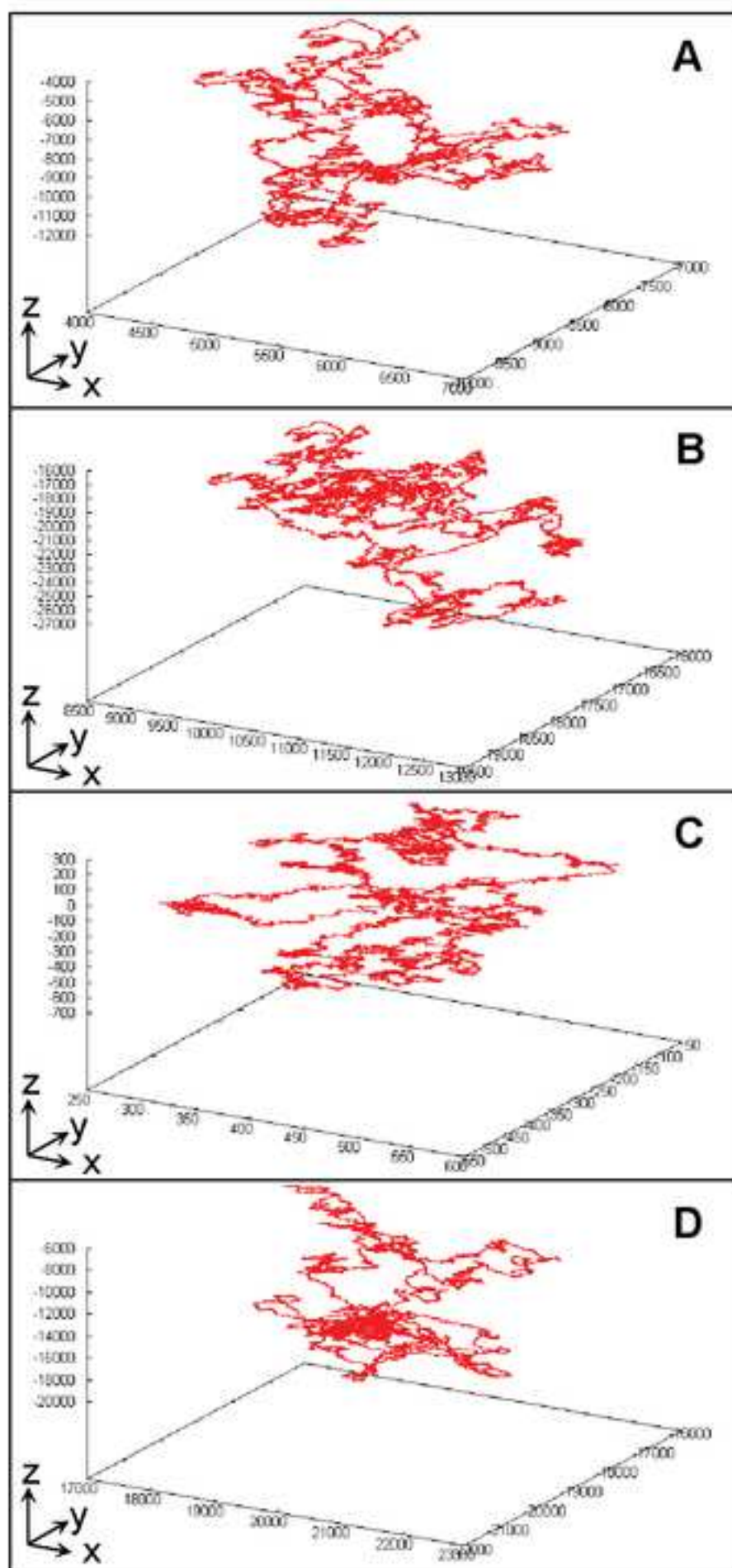
Number	<i>GenomeFingerprinter</i>		Mauve
1 chr.	1 min cal.	1 min plot	no valid
2 chr.	2 min cal.	2 min plot	2 min
4 chr.	4 min cal.	4 min plot	8 min
8 chr.	8 min cal.	8 min plot	44 min
16 chr.	16 min cal.	16 min plot	332 min
32 chr.	32 min cal.	32 min plot	MO

* Notes:

- 1) MO: memory overflow;
- 2) Samples: 32 chromosomes (chr.) as list (*) in Table 2;
- 3) Conditions: HP Proliant server DL580-G5 with 16 CPU/8Gb memory.

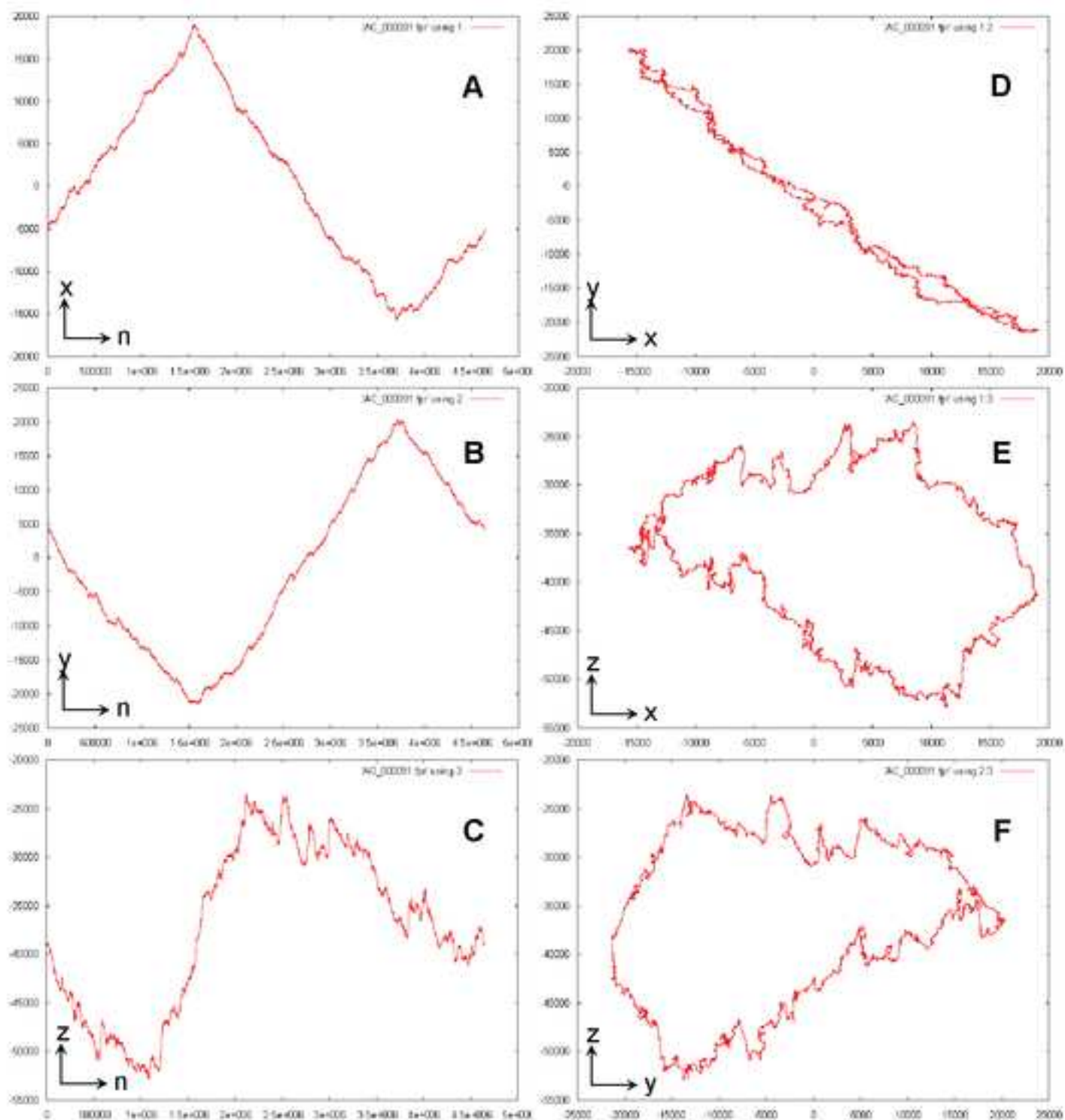
Figure

[Click here to download high resolution image](#)



Figure

[Click here to download high resolution image](#)



Figure

[Click here to download high resolution image](#)

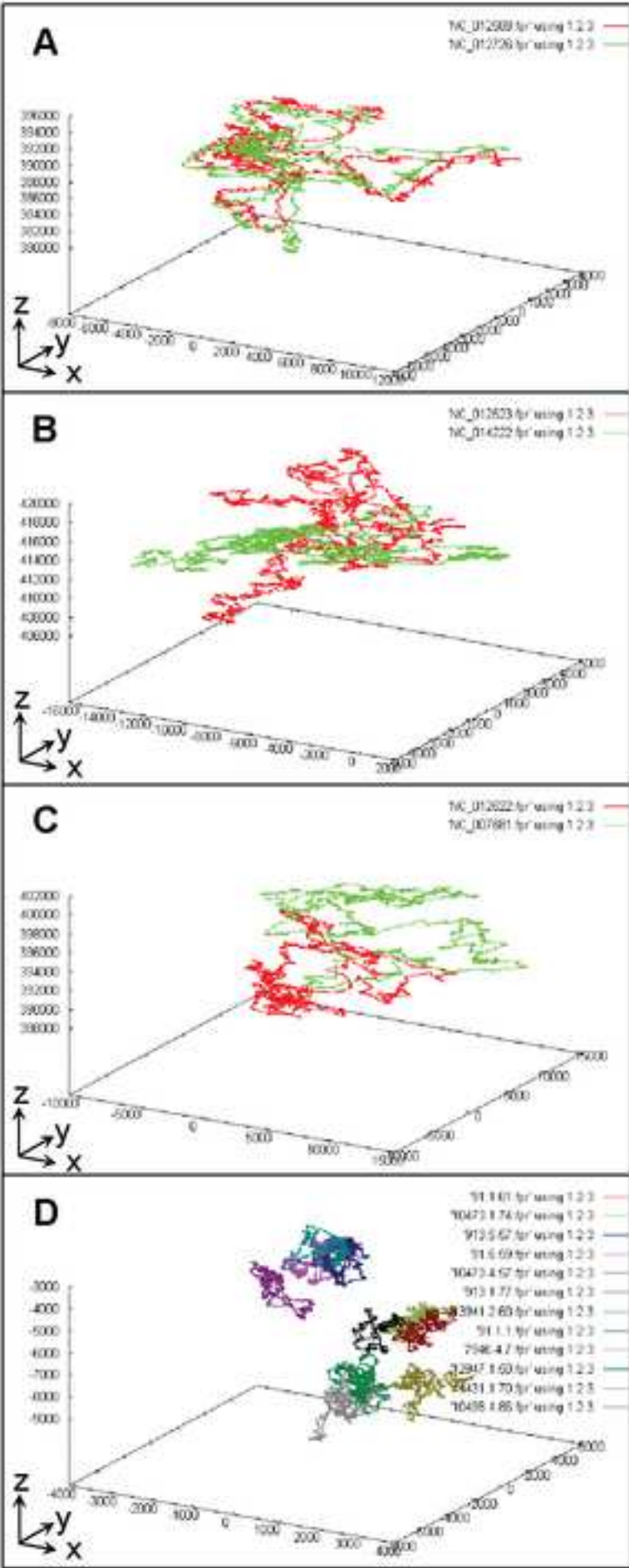


Figure
[Click here to download high resolution image](#)

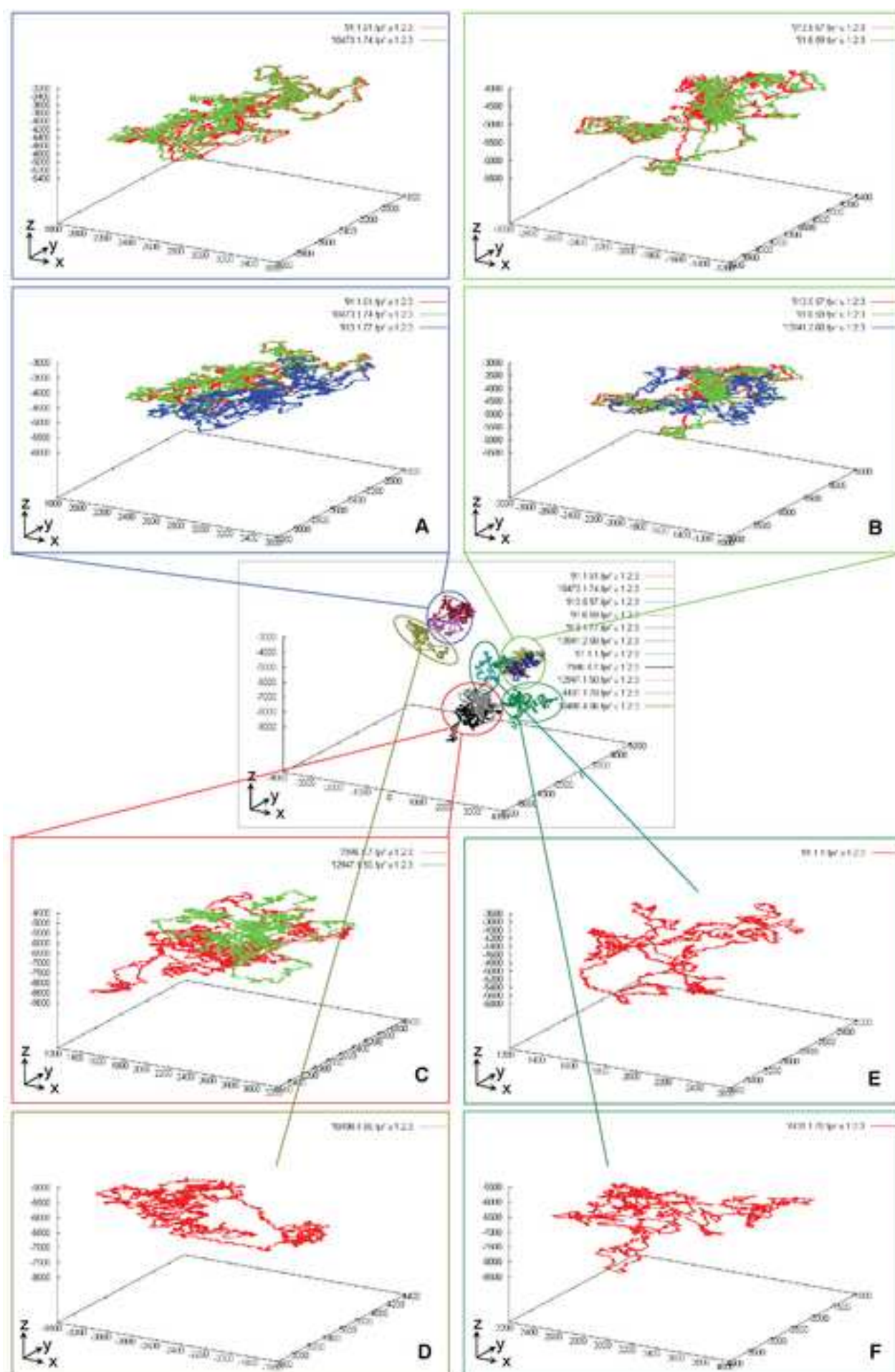
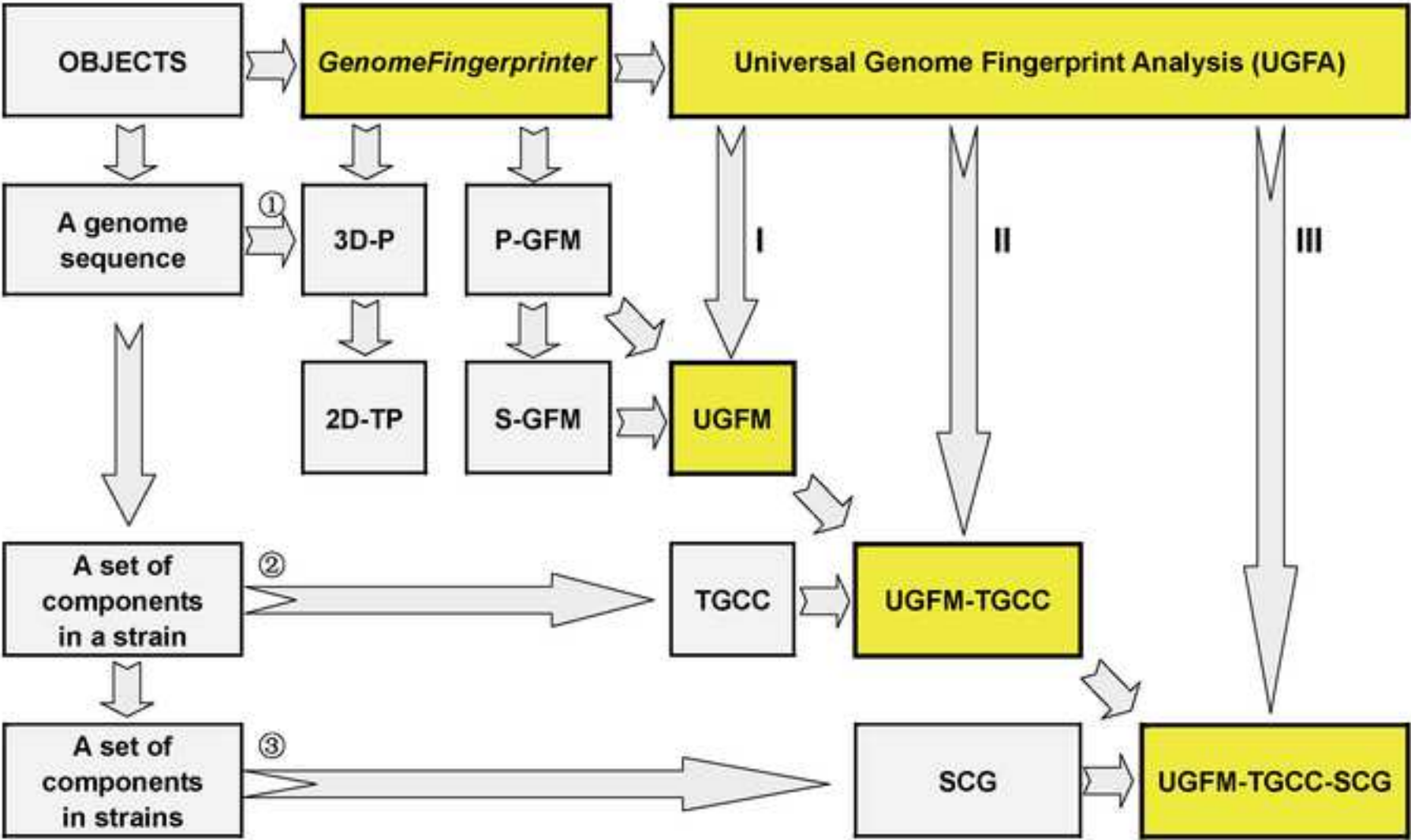
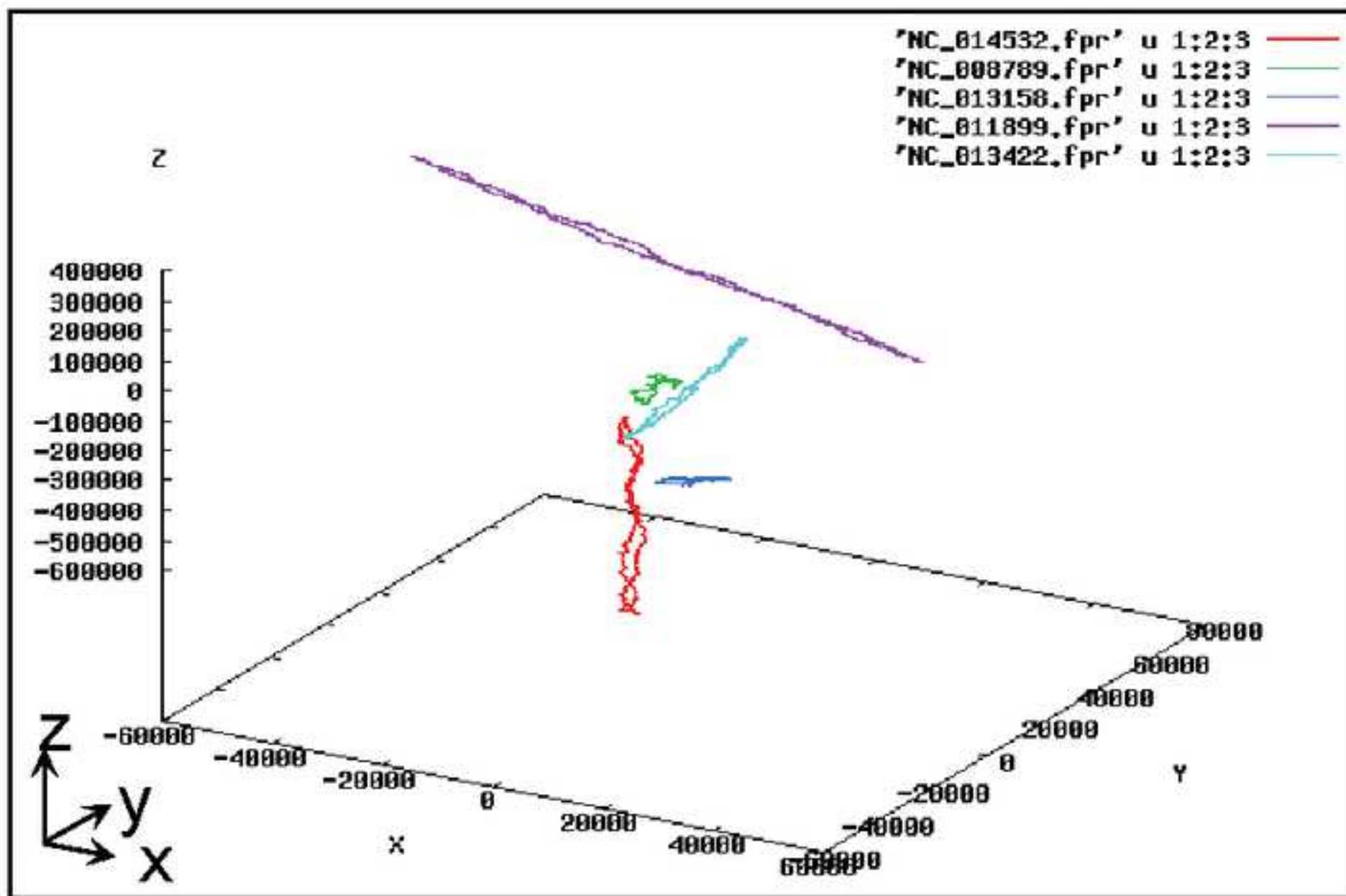


Figure
[Click here to download high resolution image](#)

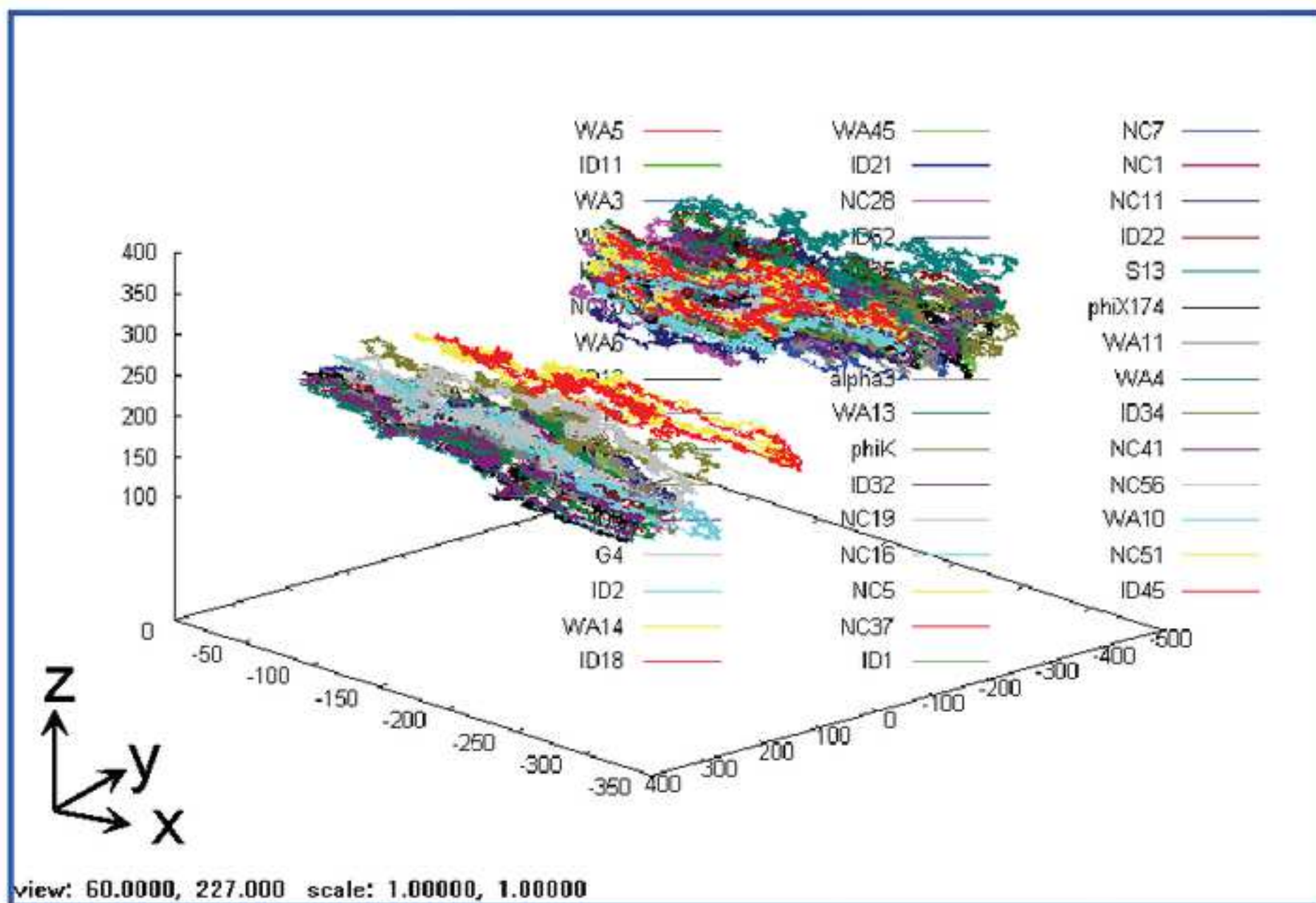


Figure

[Click here to download high resolution image](#)

Figure

[Click here to download high resolution image](#)



Figure

[Click here to download high resolution image](#)

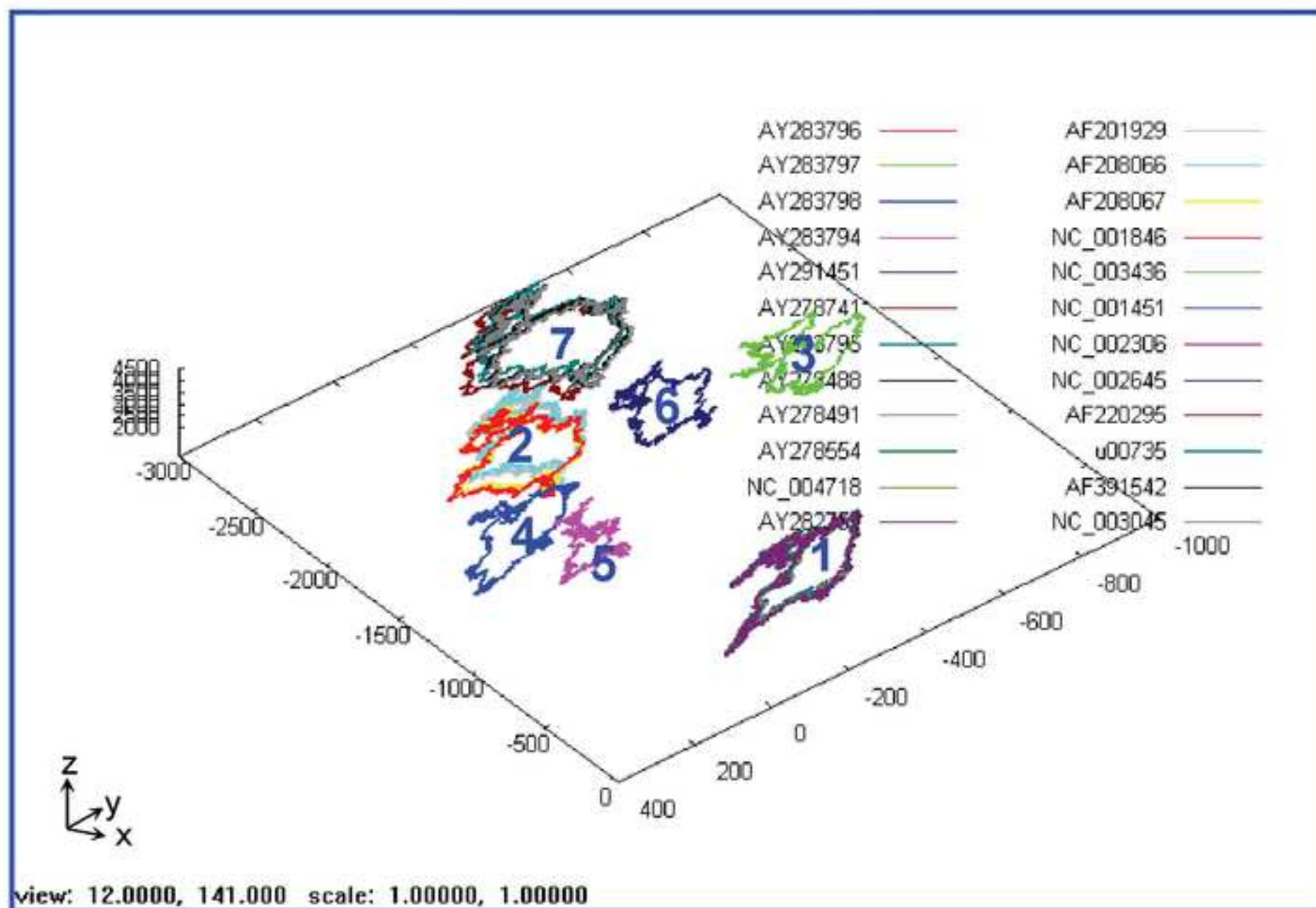


Figure
[Click here to download high resolution image](#)

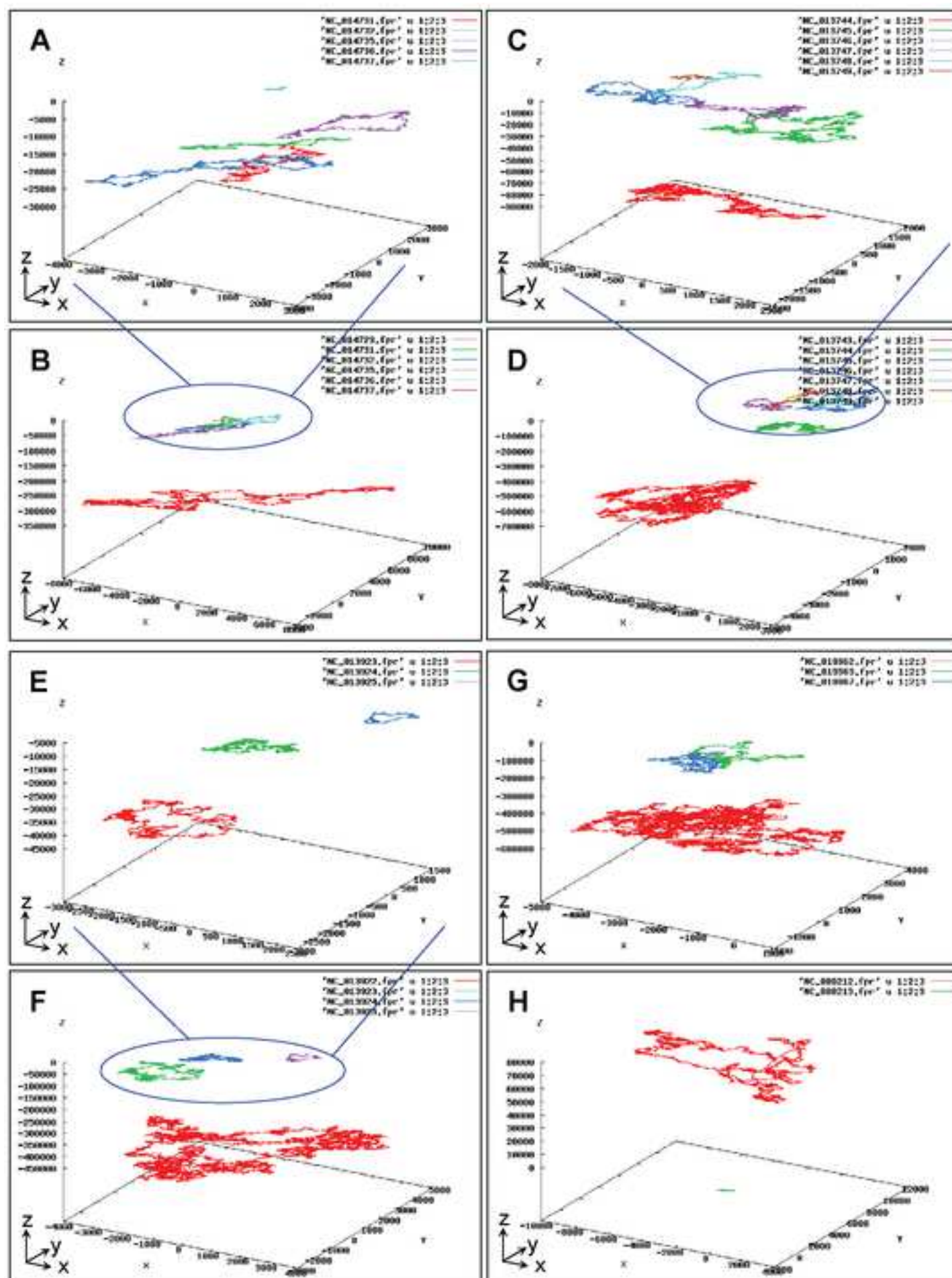


Figure
[Click here to download high resolution image](#)

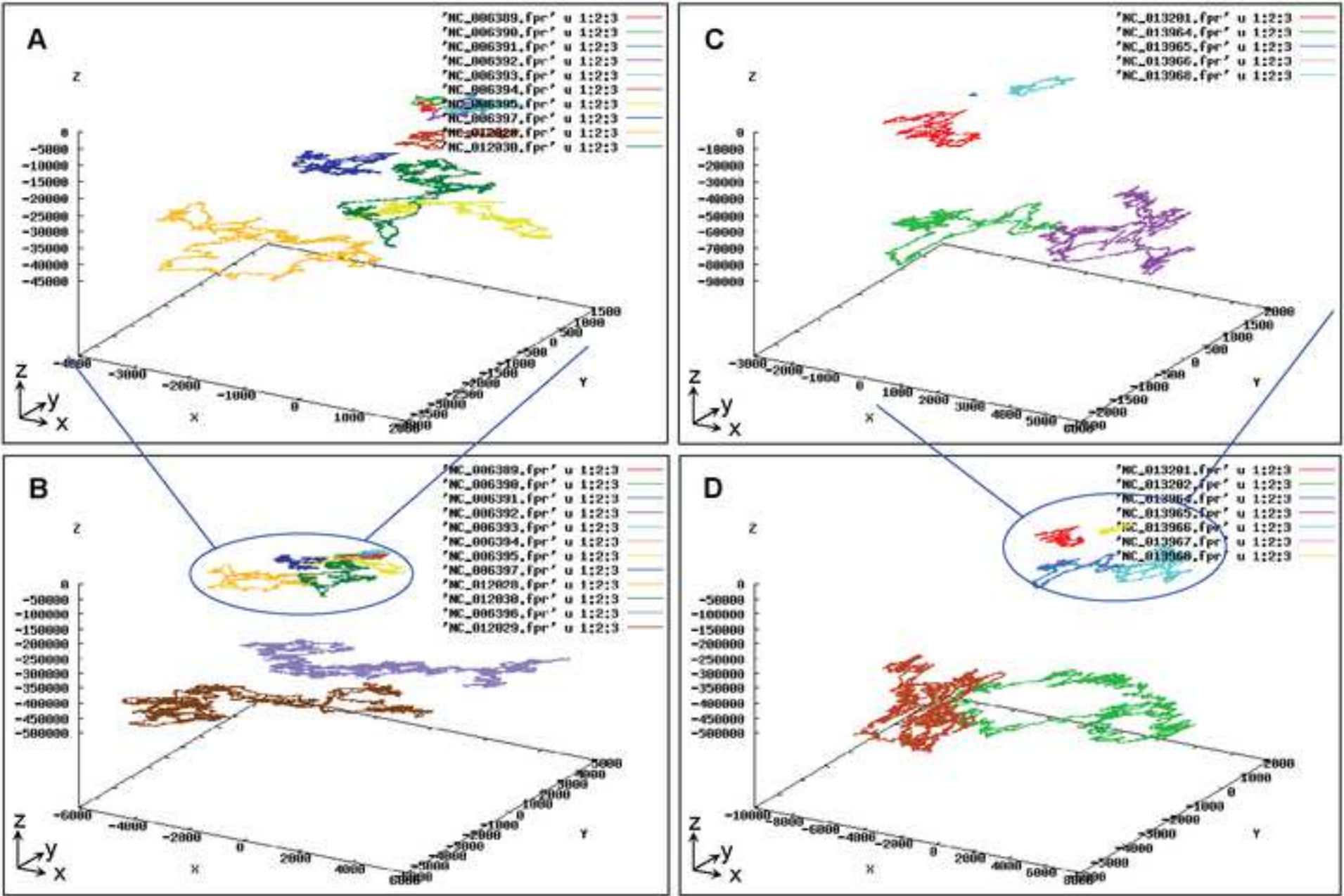


Figure
[Click here to download high resolution image](#)

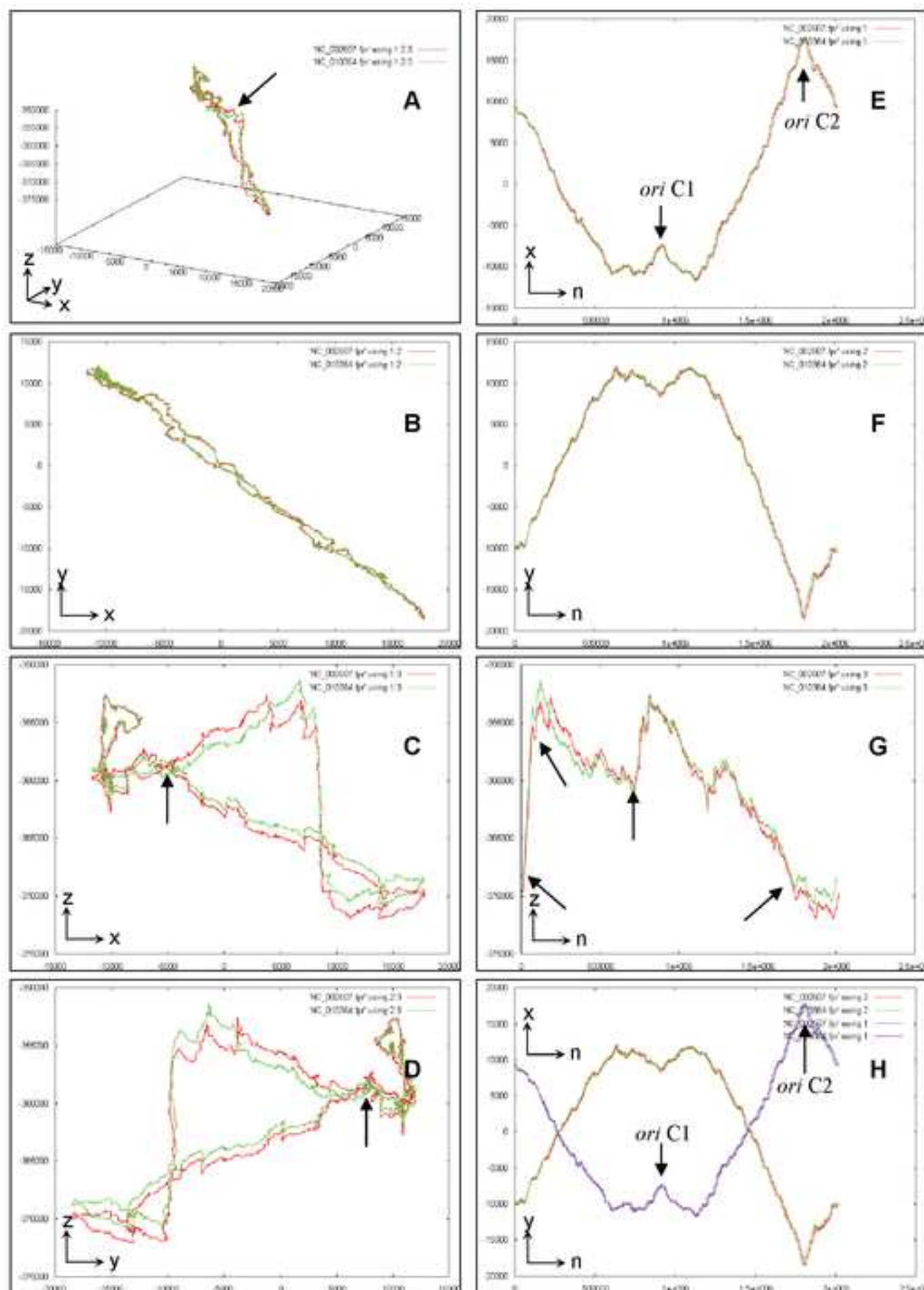


Figure
[Click here to download high resolution image](#)

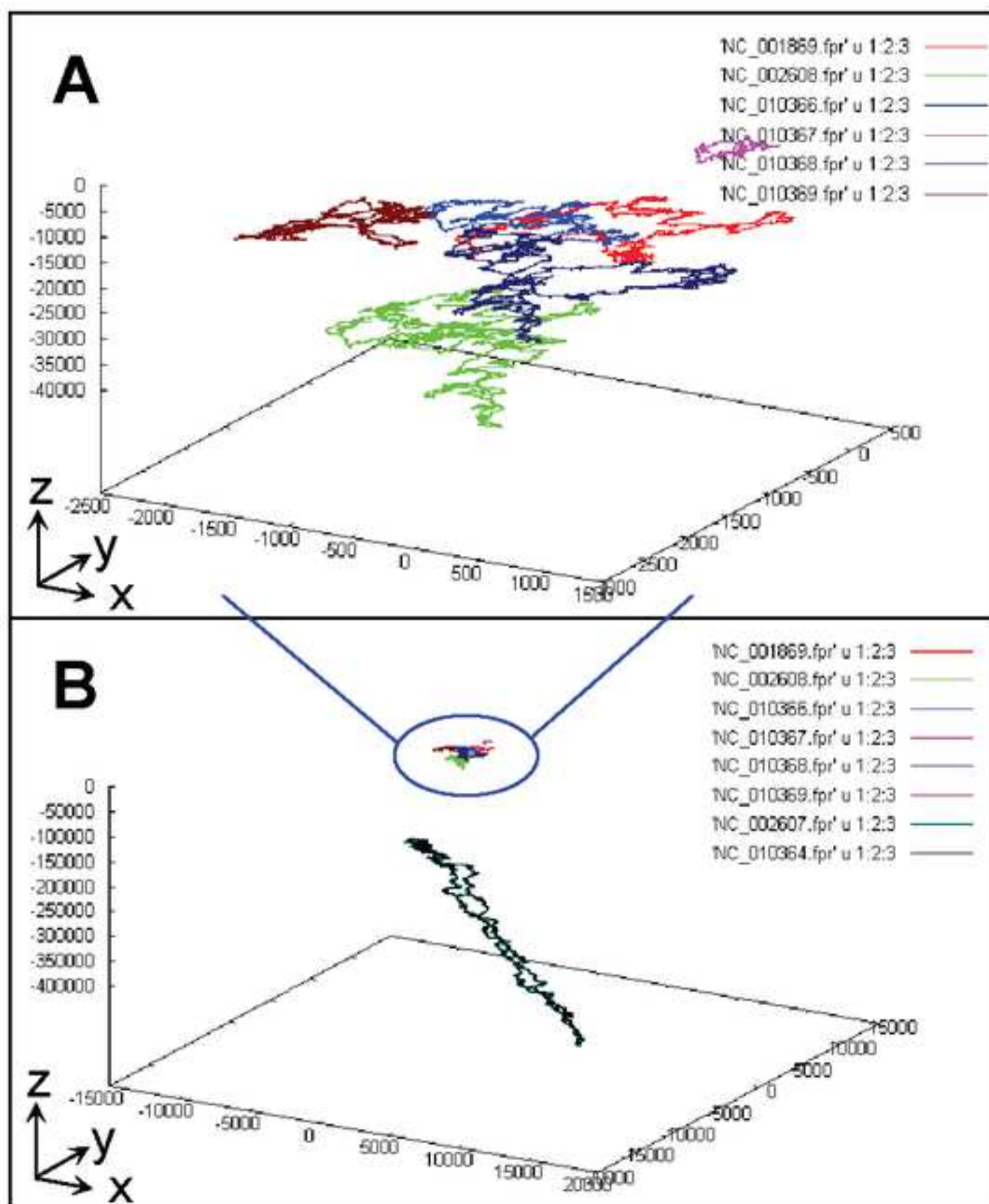
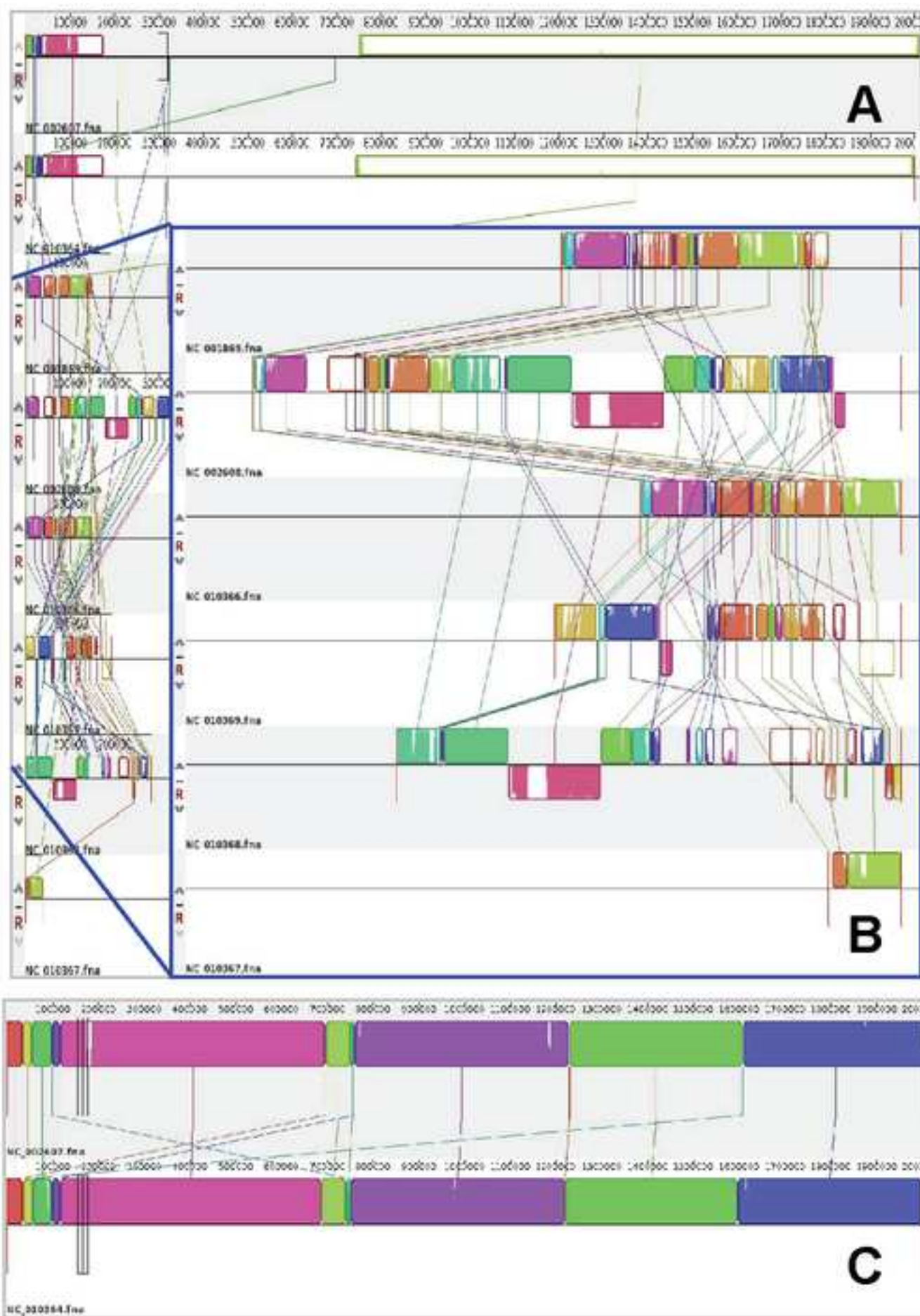


Figure
[Click here to download high resolution image](#)



Figure

[Click here to download high resolution image](#)

